A new inverse trigonometric shear deformation theory for isotropic and functionally graded sandwich plates

Van-Hau Nguyen[a], Trung-Kien Nguyen[a,*], Huu-Tai Thai[b], Thuc P. Vo[c]

[a] *Faculty of Civil Engineering and Applied Mechanics, University of Technical Education Ho Chi Minh City, 1 Vo Van Ngan Street, Thu Duc District, Ho Chi Minh City, Viet Nam*
[b] *Centre for Infrastructure Engineering and Safety, School of Civil and Environmental Engineering, The University of New South Wales, Sydney, NSW 2052, Australia*
[c] *Faculty of Engineering and Environment, Northumbria University, Newcastle upon Tyne, NE1 8ST, UK.*

Abstract

A new inverse trigonometric shear deformation theory is proposed for the static, buckling and free vibration analyses of isotropic and functionally graded (FG) sandwich plates. It accounts for a inverse trigonometric distribution of transverse shear stress and satisfies the traction free boundary conditions. Equations of motion obtained here are solved for three types of FG plates: FG plates, sandwich plates with FG core and sandwich plates with FG faces. Closed-form solutions are obtained to predict the deflections, stresses, critical buckling loads and natural frequencies of simply supported plates. A good agreement between the obtained predictions and the available solutions of existing shear deformation theories is found to demonstrate the accuracy of the proposed theory.

Keywords: A. Plates; B. Buckling; B. Vibration; C. Numerical Analysis

1. Introduction

Functionally graded material (FGM) is an advanced composite material, which is produced by a continuously graded variation of the volume fractions of the constituents [1]. Large applications of functionally graded (FG) structures have led the development of various plate theories to predict accurately their static, buckling and vibration behaviours. They are generally followed: classical plate theory (CPT) neglecting the transverse shear deformation effects ([2]-[7]), first-shear deformation theory (FSDT) with linear variation of displacements ([5], [8]-[14]), higher-order shear deformation theory (HSDT) with higher-order variations of displacements through the plate thickness such as third-order shear deformation plate theory (TSDT), sinusoidal shear deformation plate theory (SSDT), hyperbolic shear deformable plate theory (HDT) ([15]-[25]), quasi-3D theories taking into account

*Corresponding author, tel.: +84 (8) 38972092
Email address: kiennt@hcmute.edu.vn (Trung-Kien Nguyen)

normal stretching effect ([26]-[37]). Moreover, owing to smooth variations of material properties, FG sandwich plates have recently been developed to overcome interface problems between faces and core found in conventional sandwich structures. Many plate theories have been applied to predict responses of FG sandwich plates: static behaviours ([38]-[46]), vibration and buckling responses ([38], [45]-[53]). In higher-order shear deformation and quasi-3D theories, transverse shear stresses are refined through the thickness, and thus no shear correction factors are required. However, the accuracy of these approaches depends on the choice of a shape function, which is studied by many authors.

The objective of this paper is to propose a new inverse trigonometric shear deformation theory for static, vibration and buckling analyses of isotropic and FG sandwich plates. It accounts for a inverse trigonometric distribution of transverse shear stress and satisfies the traction free boundary conditions. Equations of motion obtained here are solved for three types of FG plates: FG plates, sandwich plates with FG core and sandwich plates with FG faces. Closed-form solutions are obtained to predict the deflections, stresses, critical buckling loads and natural frequencies of simply supported plates. A good agreement between the obtained predictions and the available solutions of existing shear deformation theories is found to demonstrate the accuracy of the proposed theory.

2. Problem formulation

Consider a rectangular plate with length a, width b and uniform thickness h. The plate is assumed to be subjected to a transverse mechanical load at the top surface and a compressive in-plane load on the mid-plane of the plate. Three different types of FG plates are considered:

2.1. Type A: isotropic FG plates

The plate of Type A is graded from metal at its bottom surface to ceramic at the top one (Fig. 1). The volume fraction of ceramic material V_c is given as follows:

$$V_c(z) = \left(\frac{2z+h}{2h}\right)^p \tag{1}$$

.

where p is the power-law index, which is positive and $z \in [-\frac{h}{2}, \frac{h}{2}]$.

2.2. Type B: sandwich plates with FG core

The core of this type is graded from metal to ceramic. The bottom face is made of isotropic metal, whereas the top face is isotropic ceramic. The vertical positions of the bottom and top surfaces, and of two interfaces between the layers are denoted by $h_0 = -\frac{h}{2}$, h_1, h_2, $h_3 = \frac{h}{2}$, respectively. h_1, h_2 vary according the thickness ratio of layers. The volume fraction function of ceramic phase $V_c^{(j)}$ defined by:

$$\begin{cases} V_c^{(1)}(z) = 0 & \text{for} \quad z \in [h_0, h_1] \\ V_c^{(2)}(z) = \left(\frac{z-h_1}{h_2-h_1}\right)^p & \text{for} \quad z \in [h_1, h_2] \\ V_c^{(3)}(z) = 1 & \text{for} \quad z \in [h_2, h_3] \end{cases} \tag{2}$$

The variation of ceramic material through the plate thickness for (1-2-1) sandwich plate of Type B is displayed in Fig. 2a.

2.3. Type C: sandwich plates with FG faces

The faces of this type are graded from metal to ceramic. The core is made of isotropic ceramic. The volume fraction function of ceramic phase $V_c^{(j)}$ given by:

$$\begin{cases} V_c^{(1)}(z) = \left(\frac{z-h_0}{h_1-h_0}\right)^p & \text{for} \quad z \in [h_0, h_1] \\ V_c^{(2)}(z) = 1 & \text{for} \quad z \in [h_1, h_2] \\ V_c^{(3)}(z) = \left(\frac{z-h_3}{h_2-h_3}\right)^p & \text{for} \quad z \in [h_2, h_3] \end{cases} \tag{3}$$

The variation of ceramic material through the plate thickness for (1-2-1) sandwich plate of Type C is displayed in Fig. 2b.

2.4. Kinematics and strains

Based on a new inverse trigonometric shear deformation theory, the following displacement field is assumed:

$$\begin{aligned} u(x,y,z) &= u_0(x,y) - z\frac{\partial w_0}{\partial x} + f(z)\theta_x(x,y) \\ v(x,y,z) &= v_0(x,y) - z\frac{\partial w_0}{\partial y} + f(z)\theta_y(x,y) \\ w(x,y,z) &= w_0(x,y) \end{aligned} \tag{4}$$

where

$$f(z) = h \arctan\frac{rz}{h} - \frac{16rz^3}{3h^2(r^2+4)} \tag{5}$$

and u_0, v_0, w_0, θ_x, θ_y are five unknown displacements of the midplane of the plate.

The strain field associated with the displacement field in Eq. (4) are written under following compact form:

$$\boldsymbol{\epsilon} = \boldsymbol{\epsilon}^{(0)} + z\boldsymbol{\epsilon}^{(1)} + f\boldsymbol{\epsilon}^{(2)} \tag{6a}$$

$$\boldsymbol{\gamma} = g\boldsymbol{\gamma}^{(0)} \tag{6b}$$

where $g = df/dz$, $\boldsymbol{\epsilon}^{(0)}$, $\boldsymbol{\epsilon}^{(1)}$, $\boldsymbol{\epsilon}^{(2)}$ and $\boldsymbol{\gamma}^{(0)}$ are membrane strains, curvatures and transverse shear strains, respectively. They are related to the displacement field in Eq. (4) as follows:

$$\boldsymbol{\epsilon}^{(0)} = \left\{ \begin{array}{c} \epsilon_{xx}^{(0)} \\ \epsilon_{yy}^{(0)} \\ \gamma_{xy}^{(0)} \end{array} \right\} = \left\{ \begin{array}{c} \frac{\partial u_0}{\partial x} \\ \frac{\partial v_0}{\partial y} \\ \frac{\partial u_0}{\partial y} + \frac{\partial v_0}{\partial x} \end{array} \right\}, \tag{7a}$$

$$\boldsymbol{\epsilon}^{(1)} = \left\{ \begin{array}{c} \epsilon_{xx}^{(1)} \\ \epsilon_{yy}^{(1)} \\ \gamma_{xy}^{(1)} \end{array} \right\} = \left\{ \begin{array}{c} -\frac{\partial^2 w_0}{\partial x^2} \\ -\frac{\partial^2 w_0}{\partial y^2} \\ -2\frac{\partial^2 w_0}{\partial x \partial y} \end{array} \right\}, \boldsymbol{\epsilon}^{(2)} = \left\{ \begin{array}{c} \epsilon_{xx}^{(2)} \\ \epsilon_{yy}^{(2)} \\ \gamma_{xy}^{(2)} \end{array} \right\} = \left\{ \begin{array}{c} \frac{\partial \theta_x}{\partial x} \\ \frac{\partial \theta_y}{\partial y} \\ \frac{\partial \theta_x}{\partial y} + \frac{\partial \theta_y}{\partial x} \end{array} \right\} \tag{7b}$$

$$\boldsymbol{\gamma}^{(0)} = \left\{ \begin{array}{c} \gamma_{xz}^{(0)} \\ \gamma_{yz}^{(0)} \end{array} \right\} = \left\{ \begin{array}{c} \theta_x \\ \theta_y \end{array} \right\} \tag{7c}$$

2.5. Equations of motion

Using Hamiltons principle derives the equation of motion:

$$0 = \int_0^T (\delta U + \delta V - \delta K)\, dt \tag{8}$$

where δU, δV, δK are the variations of strain energy, work done, and kinetic energy of the plate, respectively.

The variation of strain energy is calculated by:

$$\begin{aligned} \delta U &= \int_A \int_{-h/2}^{h/2} (\sigma_{xx}\delta\epsilon_{xx} + \sigma_{yy}\delta\epsilon_{yy} + \sigma_{xy}\delta\gamma_{xy} + \sigma_{xz}\delta\gamma_{xz} + \sigma_{yz}\delta\gamma_{yz})\, dA\, dz \\ &= \int_A \left[N_{xx}\frac{\partial \delta u_0}{\partial x} - M_{xx}\frac{\partial^2 \delta w_0}{\partial x^2} + R_{xx}\frac{\partial \delta \theta_x}{\partial x} + N_{yy}\frac{\partial \delta v_0}{\partial y} - M_{yy}\frac{\partial^2 \delta w_0}{\partial y^2} - R_{yy}\frac{\partial \delta \theta_y}{\partial y} \right. \\ &+ \left. N_{xy}\left(\frac{\partial \delta u_0}{\partial y} + \frac{\partial \delta v_0}{\partial x}\right) - 2M_{xy}\frac{\partial^2 \delta w_0}{\partial x \partial y} + R_{xy}\left(\frac{\partial \delta \theta_x}{\partial y} + \frac{\partial \delta \theta_y}{\partial x}\right) + Q_x\delta\theta_x + Q_y\delta\theta_y \right] dA \end{aligned} \tag{9}$$

where N, M, R, and Q are the stress resultants defined by:

$$(N_{xx}, N_{yy}, N_{xy}) = \int_{-h/2}^{h/2} (\sigma_{xx}, \sigma_{yy}, \sigma_{xy})\, dz \tag{10a}$$

$$(M_{xx}, M_{yy}, M_{xy}) = \int_{-h/2}^{h/2} z\,(\sigma_{xx}, \sigma_{yy}, \sigma_{xy})\, dz \tag{10b}$$

$$(R_{xx}, R_{yy}, R_{xy}) = \int_{-h/2}^{h/2} f\,(\sigma_{xx}, \sigma_{yy}, \sigma_{xy})\, dz \tag{10c}$$

$$(Q_x, Q_y) = \int_{-h/2}^{h/2} g(\sigma_{xz}, \sigma_{yz})\, dz \tag{10d}$$

The variation of work done by in-plane and transverse loads is given by:

$$\delta V = -\int_A \bar{N}\delta w_0 dA - \int_A q\delta w_0 dA \tag{11}$$

where

$$\bar{N} = N^0_{xx}\frac{\partial^2 w_0}{\partial x^2} + 2N^0_{xy}\frac{\partial^2 w_0}{\partial x \partial y} + N^0_{yy}\frac{\partial^2 w_0}{\partial y^2} \tag{12}$$

The variation of kinetic energy is determined by:

$$\begin{aligned}
\delta K &= \int_A \int_{-h/2}^{h/2} (\dot{u}\delta\dot{u} + \dot{v}\delta\dot{v} + \dot{w}\delta\dot{w})\rho(z)\, dz\, dA \\
&= \int_A \Bigg\{ I_0 \left(\dot{u}_0\delta\dot{u}_0 + \dot{v}_0\delta\dot{v}_0 + \dot{w}_0\delta\dot{w}_0\right) - I_1 \left(\dot{u}_0\frac{\partial\delta\dot{w}_0}{\partial x} + \frac{\partial\dot{w}_0}{\partial x}\delta\dot{u}_0 + \dot{v}_0\frac{\partial\delta\dot{w}_0}{\partial y} + \frac{\partial\dot{w}_0}{\partial y}\delta\dot{v}_0\right) \\
&+ I_2 \left(\frac{\partial\dot{w}_0}{\partial x}\frac{\partial\delta\dot{w}_0}{\partial x} + \frac{\partial\dot{w}_0}{\partial y}\frac{\partial\delta\dot{w}_0}{\partial y}\right) + J_1 \left(\dot{u}_0\delta\dot{\theta}_x + \dot{\theta}_x\delta\dot{u}_0 + \dot{v}_0\delta\dot{\theta}_y + \dot{\theta}_y\delta\dot{v}_0\right) \\
&+ K_2 \left(\dot{\theta}_x\delta\dot{\theta}_x + \dot{\theta}_y\delta\dot{\theta}_y\right) - J_2 \left(\frac{\partial\dot{w}_0}{\partial x}\delta\dot{\theta}_x + \dot{\theta}_x\frac{\partial\delta\dot{w}_0}{\partial x} + \frac{\partial\dot{w}_0}{\partial y}\delta\dot{\theta}_y + \dot{\theta}_y\frac{\partial\delta\dot{w}_0}{\partial y}\right)\Bigg\}\, dA
\end{aligned} \tag{13}$$

where the dot-superscript convention indicates the differentiation with respect to the time variable t, $\rho(z)$ is the mass density, and the inertia terms I_i, J_i, K_i are expressed by:

$$(I_0, I_1, I_2) = \int_{-h/2}^{h/2} (1, z, z^2)\rho(z) dz \tag{14a}$$

$$(J_1, J_2, K_2) = \int_{-h/2}^{h/2} (f, zf, f^2)\rho(z) dz \tag{14b}$$

Substituting Eqs. (9), (11), and (13) into Eq. (8), integrating by parts, and collecting the coeffi-

cients of δu_0, δv_0, δw_0, $\delta\theta_x$, $\delta\theta_y$, equations of motion are obtained:

$$\delta u_0 \quad : \quad \frac{\partial N_{xx}}{\partial x} + \frac{\partial N_{xy}}{\partial y} = I_0\ddot{u}_0 - I_1\frac{\partial \ddot{w}_0}{\partial x} + J_1\ddot{\theta}_x \tag{15a}$$

$$\delta v_0 \quad : \quad \frac{\partial N_{xy}}{\partial x} + \frac{\partial N_{yy}}{\partial y} = I_0\ddot{v}_0 - I_1\frac{\partial \ddot{w}_0}{\partial y} + J_1\ddot{\theta}_y \tag{15b}$$

$$\begin{aligned}\delta w_0 \quad : \quad & \frac{\partial^2 M_{xx}}{\partial x^2} + 2\frac{\partial^2 M_{xy}}{\partial x \partial y} + \frac{\partial M_{yy}}{\partial y^2} + \bar{N} + q \\ = \quad & I_0\ddot{w}_0 + I_1\left(\frac{\partial \ddot{u}_0}{\partial x} + \frac{\partial \ddot{v}_0}{\partial y}\right) - I_2\nabla^2\ddot{w}_0 + J_2\left(\frac{\partial \ddot{\theta}_x}{\partial x} + \frac{\partial \ddot{\theta}_y}{\partial y}\right)\end{aligned} \tag{15c}$$

$$\delta\theta_x \quad : \quad \frac{\partial R_{xx}}{\partial x} + \frac{\partial R_{xy}}{\partial y} - Q_x = J_1\ddot{u}_0 - J_2\frac{\partial \ddot{w}_0}{\partial x} + K_2\ddot{\theta}_x \tag{15d}$$

$$\delta\theta_y \quad : \quad \frac{\partial R_{xy}}{\partial x} + \frac{\partial R_{yy}}{\partial y} - Q_y = J_1\ddot{v}_0 - J_2\frac{\partial \ddot{w}_0}{\partial y} + K_2\ddot{\theta}_y \tag{15e}$$

where $\nabla^2 = \partial^2/\partial x^2 + \partial^2/\partial y^2$ is the Laplacian operator in two-dimensional Cartesian coordinate system.

The effective material properties at the j-th layer of FG plates according to the power-law form are expressed by:

$$P^{(j)}(z) = (P_c - P_m)V_c^{(j)}(z) + P_m \tag{16}$$

where P_m and P_c are the Young's modulus (E), Poisson's ratio (ν), mass densities (ρ) of metal and ceramic materials, respectively.

For elastic and isotropic FG plates, the constitutive relations can be written as

$$\left\{\begin{array}{c}\sigma_{xx}\\ \sigma_{yy}\\ \sigma_{xy}\end{array}\right\} = \left[\begin{array}{ccc}C_{11} & C_{12} & 0\\ C_{12} & C_{22} & 0\\ 0 & 0 & C_{66}\end{array}\right]\left\{\begin{array}{c}\epsilon_{xx}\\ \epsilon_{yy}\\ \gamma_{xy}\end{array}\right\} \tag{17a}$$

$$\left\{\begin{array}{c}\sigma_{xz}\\ \sigma_{yz}\end{array}\right\} = \left[\begin{array}{cc}C_{55} & 0\\ 0 & C_{44}\end{array}\right]\left\{\begin{array}{c}\gamma_{xz}\\ \gamma_{yz}\end{array}\right\} \tag{17b}$$

where

$$C_{11}(z) = C_{22}(z) = \frac{E(z)}{1-\nu(z)^2}, C_{12}(z) = \nu(z)C_{11}(z) \tag{18a}$$

$$C_{44}(z) = C_{55}(z) = C_{66}(z) = \frac{E(z)}{2(1+\nu(z))} \tag{18b}$$

Substituting Eq. (7b) into Eq. (17a) and the subsequent results into Eqs. (10a), (10b) and (10c),

the stress resultants are obtained in terms of strains as following compact form:

$$\left\{ \begin{array}{c} \mathbf{N} \\ \mathbf{M} \\ \mathbf{R} \end{array} \right\} = \left[\begin{array}{ccc} \mathbf{A} & \mathbf{B} & \mathbf{B}^s \\ \mathbf{B} & \mathbf{D} & \mathbf{D}^s \\ \mathbf{B}^s & \mathbf{D}^s & \mathbf{H}^s \end{array} \right] \left\{ \begin{array}{c} \boldsymbol{\epsilon}^{(0)} \\ \boldsymbol{\epsilon}^{(1)} \\ \boldsymbol{\epsilon}^{(2)} \end{array} \right\} \tag{19}$$

where $\mathbf{A}, \mathbf{B}, \mathbf{D}, \mathbf{B}^s, \mathbf{D}^s, \mathbf{H}^s$ are the stiffnesses of the FG plate given by:

$$(\mathbf{A}, \mathbf{B}, \mathbf{D}, \mathbf{B}^s, \mathbf{D}^s, \mathbf{H}^s) = \int_{-h/2}^{h/2} (1, z, z^2, f, zf, f^2) \mathbf{C}(z) dz \tag{20}$$

Similarly, using Eqs. (7c), (17b) and (10d), the transverse shear forces can be calculated from the constitutive equations as:

$$\left\{ \begin{array}{c} Q_x \\ Q_y \end{array} \right\} = \left[\begin{array}{cc} A^s_{55} & 0 \\ 0 & A^s_{44} \end{array} \right] \left\{ \begin{array}{c} \gamma^{(0)}_{xz} \\ \gamma^{(0)}_{yz} \end{array} \right\} \tag{21}$$

or in a compact form as:

$$\mathbf{Q} = \mathbf{A}^s \boldsymbol{\gamma}^0 \tag{22}$$

where the shear stiffnesses $\mathbf{A}^s$ of the FG plate are defined by:

$$A^s_{44} = A^s_{55} = \int_{-h/2}^{h/2} g^2(z) C_{44}(z) dz = \int_{-h/2}^{h/2} g^2(z) C_{55}(z) dz \tag{23}$$

By substituting Eqs. (19) and (22) into Eq. (15), the equations of motion can be expressed in

terms of displacements $(u_0, v_0, w_0, \theta_x, \theta_y)$ as follows:

$$A_{11}\frac{\partial^2 u_0}{\partial x^2} + A_{66}\frac{\partial^2 u_0}{\partial y^2} + (A_{12}+A_{66})\frac{\partial^2 v_0}{\partial x \partial y} - B_{11}\frac{\partial^3 w_0}{\partial x^3} - (B_{12}+2B_{66})\frac{\partial^3 w_0}{\partial x \partial y^2} + B_{11}^s\frac{\partial^2 \theta_x}{\partial x^2} + B_{66}^s\frac{\partial^2 \theta_x}{\partial y^2} + (B_{12}^s + B_{66}^s)\frac{\partial^2 \theta_y}{\partial x \partial y} = I_0\ddot{u}_0 - I_1\frac{\partial \ddot{w}_0}{\partial x} + J_1\ddot{\theta}_x \quad (24a)$$

$$A_{22}\frac{\partial^2 v_0}{\partial y^2} + A_{66}\frac{\partial^2 v_0}{\partial x^2} + (A_{12}+A_{66})\frac{\partial^2 u_0}{\partial x \partial y} - B_{22}\frac{\partial^3 w_0}{\partial y^3} - (B_{12}+2B_{66})\frac{\partial^3 w_0}{\partial x^2 \partial y} + B_{22}^s\frac{\partial^2 \theta_y}{\partial y^2} + B_{66}^s\frac{\partial^2 \theta_y}{\partial x^2} + (B_{12}^s + B_{66}^s)\frac{\partial^2 \theta_x}{\partial x \partial y} = I_0\ddot{v}_0 - I_1\frac{\partial \ddot{w}_0}{\partial y} + J_1\ddot{\theta}_y \quad (24b)$$

$$B_{11}\frac{\partial^3 u_0}{\partial x^3} + (B_{12}+2B_{66})\frac{\partial^3 u_0}{\partial x \partial y^2} + (B_{12}+2B_{66})\frac{\partial^3 v_0}{\partial x^2 \partial y} + B_{22}\frac{\partial^3 v_0}{\partial y^3} - D_{11}\frac{\partial^4 w_0}{\partial x^4} - D_{22}\frac{\partial^4 w_0}{\partial y^4} - 2(D_{12}+2D_{66})\frac{\partial^4 w_0}{\partial x^2 \partial y^2} + D_{11}^s\frac{\partial^3 \theta_x}{\partial x^3} + D_{22}^s\frac{\partial^3 \theta_y}{\partial y^3} + (D_{12}^s + 2D_{66}^s)\frac{\partial^3 \theta_x}{\partial x \partial y^2} + (D_{12}^s + 2D_{66}^s)\frac{\partial^3 \theta_y}{\partial x^2 \partial y} + \bar{N}(w) + q = I_0\ddot{w}_0 + I_1\left(\frac{\partial \ddot{u}_0}{\partial x} + \frac{\partial \ddot{v}_0}{\partial y}\right) - I_2\nabla^2\ddot{w}_0 + J_2\left(\frac{\partial \ddot{\theta}_x}{\partial x} + \frac{\partial \ddot{\theta}_y}{\partial y}\right) \quad (24c)$$

$$B_{11}^s\frac{\partial^2 u_0}{\partial x^2} + (B_{12}^s + B_{66}^s)\frac{\partial^2 v_0}{\partial x \partial y} + B_{66}^s\frac{\partial^2 u_0}{\partial y^2} - D_{11}^s\frac{\partial^3 w_0}{\partial x^3} - (D_{12}^s + 2D_{66}^s)\frac{\partial^3 w_0}{\partial x \partial y^2} - A_{55}^s\theta_x + H_{11}^s\frac{\partial^2 \theta_x}{\partial x^2} + (H_{12}^s + H_{66}^s)\frac{\partial^2 \theta_y}{\partial x \partial y} + H_{66}^s\frac{\partial^2 \theta_x}{\partial y^2} = J_1\ddot{u}_0 - J_2\frac{\partial \ddot{w}_0}{\partial x} + K_2\ddot{\theta}_x \quad (24d)$$

$$B_{22}^s\frac{\partial^2 v_0}{\partial y^2} + (B_{12}^s + B_{66}^s)\frac{\partial^2 u_0}{\partial x \partial y} + B_{66}^s\frac{\partial^2 v_0}{\partial x^2} - D_{22}^s\frac{\partial^3 w_0}{\partial y^3} - (D_{12}^s + 2D_{66}^s)\frac{\partial^3 w_0}{\partial x^2 \partial y} - A_{44}^s\theta_y + H_{22}^s\frac{\partial^2 \theta_y}{\partial y^2} + (H_{12}^s + H_{66}^s)\frac{\partial^2 \theta_x}{\partial x \partial y} + H_{66}^s\frac{\partial^2 \theta_y}{\partial x^2} = J_1\ddot{v}_0 - J_2\frac{\partial \ddot{w}_0}{\partial y} + K_2\ddot{\theta}_y \quad (24e)$$

2.6. Analytical solution for simply-supported FG plates

By using the Navier solution procedure, the displacement functions that are assumed to satisfy the boundary conditions are given as follows:

$$u_0(x,y,t) = \sum_{m=1}^{\infty}\sum_{n=1}^{\infty} u_{mn}\cos\lambda x\,\sin\mu y\,e^{i\omega t} \quad (25a)$$

$$v_0(x,y,t) = \sum_{m=1}^{\infty}\sum_{n=1}^{\infty} v_{mn}\sin\lambda x\,\cos\mu y\,e^{i\omega t} \quad (25b)$$

$$w_0(x,y,t) = \sum_{m=1}^{\infty}\sum_{n=1}^{\infty} w_{mn}\sin\lambda x\,\sin\mu y\,e^{i\omega t} \quad (25c)$$

$$\theta_x(x,y,t) = \sum_{m=1}^{\infty}\sum_{n=1}^{\infty} x_{mn}\cos\lambda x\,\sin\mu y\,e^{i\omega t} \quad (25d)$$

$$\theta_y(x,y,t) = \sum_{m=1}^{\infty}\sum_{n=1}^{\infty} y_{mn}\sin\lambda x\,\cos\mu y\,e^{i\omega t} \quad (25e)$$

where $\lambda = m\pi/a$, $\mu = n\pi/b$, ω is the frequency of free vibration of the plate, $\sqrt{i} = -1$ the imaginary unit. The transverse load q is also expanded in the double-Fourier sine series as:

$$q(x,y) = \sum_{m=1}^{\infty}\sum_{n=1}^{\infty} q_{mn} \sin\lambda x \, \sin\mu y \tag{26}$$

where q_{mn}=q_0 for sinusoidally distributed load. Assuming that the plate is subjected to in-plane compressive loads of form: $N^0_{xx} = -N_0$, $N^0_{yy} = -\gamma N_0$ (here γ is non-dimensional load parameter), $N^0_{xy} = 0$. Substituting Eqs. (25) and (26) into Eq. (24), the following problem is obtained:

$$\left(\begin{bmatrix} k_{11} & k_{12} & k_{13} & k_{14} & k_{15} \\ k_{12} & k_{22} & k_{23} & k_{24} & k_{25} \\ k_{13} & k_{23} & k_{33}+\alpha & k_{34} & k_{35} \\ k_{14} & k_{24} & k_{34} & k_{44} & k_{45} \\ k_{15} & k_{25} & k_{35} & k_{45} & k_{55} \end{bmatrix} - \omega^2 \begin{bmatrix} m_{11} & 0 & m_{13} & m_{14} & 0 \\ 0 & m_{22} & m_{23} & 0 & m_{25} \\ m_{13} & m_{23} & m_{33} & m_{34} & m_{35} \\ m_{14} & 0 & m_{34} & m_{44} & 0 \\ 0 & m_{25} & m_{35} & 0 & m_{55} \end{bmatrix} \right) \begin{Bmatrix} u_{mn} \\ v_{mn} \\ w_{mn} \\ x_{mn} \\ y_{mn} \end{Bmatrix} = \begin{Bmatrix} 0 \\ 0 \\ q_{mn} \\ 0 \\ 0 \end{Bmatrix} \tag{27}$$

where

$$\begin{aligned}
&k_{11} = A_{11}\lambda^2 + A_{66}\mu^2, k_{12} = (A_{12}+A_{66})\lambda\mu, k_{13} = -B_{11}\lambda^3 - (B_{12}+2B_{66})\lambda\mu^2 \\
&k_{14} = B^s_{11}\lambda^2 + B^s_{66}\mu^2, k_{15} = (B^s_{12}+B^s_{66})\lambda\mu, k_{22} = A_{66}\lambda^2 + A_{22}\mu^2 \\
&k_{23} = -B_{22}\mu^3 - (B_{12}+2B_{66})\lambda^2\mu, k_{24} = (B^s_{12}+B^s_{66})\lambda\mu, k_{25} = B^s_{22}\mu^2 + B^s_{66}\lambda^2 \\
&k_{33} = D_{11}\lambda^4 + 2(D_{12}+2D_{66})\lambda^2\mu^2 + D_{22}\mu^4, k_{34} = -D^s_{11}\lambda^3 - (D^s_{12}+2D^s_{66})\lambda\mu^2 \\
&k_{35} = -D^s_{22}\mu^3 - (D^s_{12}+2D^s_{66})\lambda^2\mu, k_{44} = H^s_{11}\lambda^2 + H^s_{66}\mu^2 + A^s_{55} \\
&k_{45} = (H^s_{12}+H^s_{66})\lambda\mu, k_{55} = H^s_{66}\lambda^2 + H^s_{22}\mu^2 + A^s_{44} \\
&m_{11} = m_{22} = I_0, m_{13} = -\lambda I_1,\ m_{14} = J_1, m_{23} = -\mu I_1, m_{25} = J_1 \\
&m_{33} = I_0 + I_2(\lambda^2+\mu^2), m_{34} = -\lambda J_2, m_{35} = -\mu J_2, m_{44} = m_{55} = K_2 \\
&\alpha = -N_0(\lambda^2 + \gamma\mu^2)
\end{aligned} \tag{28}$$

Eq. (27) is a general form for bending, buckling and free vibration analysis of isotropic and FG sandwich plates under in-plane and transverse loads. In order to solve bending problem, the in-plane compressive load N_0 and mass matrix $\mathbf{M}$ are set to zeros. The critical buckling loads (N_{cr}) can be obtained from the stability problem $|K_{ij} = 0|$ while the free vibration problem is achieved by omitting both in-plane and transverse loads.

3. Numerical results and discussion

In this section, the deflections, stresses, natural frequencies and critical buckling loads of simply-supported isotropic and FG sandwich plates are presented and compared with the existing solutions to

verify the accuracy of the proposed theory. Two material combinations of metal and ceramic: Al/ZrO_2 and Al/Al_2O_3 are considered. Their material properties are given in Table 1. For convenience, the following non-dimensional parameters are used:

$$\begin{aligned}
\bar{u}(z) &= \frac{100h^3E_c}{a^4q_0}u\left(0,\frac{b}{2},z\right), \bar{w} = \frac{10h^3E_c}{a^4q_0}w\left(\frac{a}{2},\frac{b}{2}\right), \hat{w} = \frac{10hE_0}{a^2q_0}w\left(\frac{a}{2},\frac{b}{2}\right), \quad E_0 = 1\,\text{GPa} \\
\bar{\sigma}_{xx}(z) &= \frac{h}{aq_0}\sigma_{xx}\left(\frac{a}{2},\frac{b}{2},z\right), \hat{\sigma}_{xx}(z) = \frac{10h^2}{a^2q_0}\sigma_{xx}\left(\frac{a}{2},\frac{b}{2},z\right) \\
\bar{\sigma}_{xy}(z) &= \frac{h}{aq_0}\sigma_{xx}\left(0,0,z\right), \bar{\sigma}_{xz}(z) = \frac{h}{aq_0}\sigma_{xz}\left(0,\frac{b}{2},z\right) \\
\bar{N}_{cr} &= \frac{N_{cr}a^2}{E_mh^3}, \hat{N}_{cr} = \frac{N_{cr}a^2}{100E_0h^3}, \bar{\omega} = \frac{\omega ab}{\pi^2h}\sqrt{\frac{12(1-\nu_c^2)\rho_c}{E_c}}, \hat{\omega} = \frac{\omega a^2}{h}\sqrt{\frac{\rho_0}{E_0}}, \quad \rho_o = 1\,\text{kg/m}^3
\end{aligned} \tag{29}$$

It is noted that the present solution depends on the choice of parameter r of the shape function $f(z)$. In this paper, the optimized value is determined by a postprocessing technique based on comparisons the results of the static, buckling and vibration responses obtained from present study and those of quasi-3D and 3D theories. Figure 3 presents one particular case of variations of transverse shear stresses and fundamental frequency of three types of FG plates for various values of the parameter r. From this figure, it can be seen that the minimum errors between the present solutions with those obtained by quasi-3D and 3D theories are reached for the value of $r = 1$, thus, this value will be used in this paper.

3.1. Results of bending analysis

Example 1: In the first example, the center deflections, in-plane and transverse shear stresses of Al/Al_2O_3 square plates of Type A under sinusoidal loads are calculated in Table 2. The present results are in close agreement with various shear deformation theories (SSDT [20], TSDT [23], HSDT [25], quasi-3D ([26] and [27])). The variations of transverse displacement, in-plane and out-of-plane stresses through the plate thickness are displayed in Fig. 4. It is clear that the maximum axial stress increases with p while it appears minimum compressive stresses located inside of the plate for some values of p ($p \leq 1$). The maximum shear stress is located at the mid-plane for homogeneous plates and tends to lightly move to the upper surface with respect to p, which is asymmetric characteristic of FGM through the plate thickness.

Example 2: This example aims to study the bending responses of a (1-8-1) Al/Al_2O_3 square sandwich plate of Type B. The obtained results are compared with earlier works (FSDT [40] and quasi-3D ([29], [38], [43])) in Table 3. It can be seen that the present solutions are found to be in very good agreement with the existing ones. A good agreement between the present solutions and

references considered, especially with quasi-3D theories is found. The variation of axial and transverse shear stresses through the plate thickness for various values of the power-law index is plotted in Figs. 5a and 5b.

Example 3: The next example is to consider static responses of Al/ZrO_2 sandwich plates of Type C for different skin-core-skin thickness ratios. Tables 4-6 present the center deflections, axial and transverse shear stresses of plates. The deflections increase with the increase of power-law index. It can be seen from these tables that present results are better predictions with quasi-3D ones ([38], [45]) than TSDT and SSDT ones in many cases, which again proves the accuracy of the present model in predicting the static behaviours. The variations of axial and shear stress through the thickness are displayed in Figs. 5c and 5d. It shows that the maximum stresses are located at the interfaces of layers (Fig. 5c). As expected, the maximum shear stresses is occurred at the mid-plane of (1-2-1) plate.

3.2. Results of vibration and buckling analysis

Example 4: The fundamental frequencies and critical buckling loads of Al/Al_2O_3 plates of Type A are given in Tables 7 and 8. The results presented in Table 8 are calculated for various configurations of plate with two types of in-plane loads: uniaxial compression (γ=0) and biaxial compressions (γ=1). The present solutions are compared to those obtained by a TSDT [24] and a 3D model [37]. A good agreements between these models are found, even for thick plates. For example, for $a/h = 2$, the maximum error between present solutions with 3D ones in Table 7 is 1.19% at $p = 1$ and decreases with the increase of a/h ratio. The fundamental frequencies and critical buckling loads increase with a/h and decrease with an increase of p.

Example 5: The objective of this example is to demonstrate the validity of the model in predicting vibration responses of Al/Al_2O_3 sandwich plates of Type B. It should be noted in this case, plates are composed of a mixture of metal located at the top surface and ceramic at the bottom one. The results are calculated for three side-to-thickness ratios a/h=5, 10 and 100 and three skin-core-skin thicknesses (1-1-1,1-2-1 and 2-2-1). Excellent correlation is observed between the fundamental frequency obtained from the present study and that of HSDTs [52] (HSDT9 and HSDT13 are the HSDT plate models with 9 and 13 unknowns, respectively) in Table 9. Figure 7 plots displacement shapes through the plate thickness for six vibration modes of (1-2-1) square sandwich plate with (a/h=10, p=5) and at ($x = a/4$, $y = b/4$). It can be seen that at location considered, uniform transverse deflected shapes are appeared in the modes whereas the in-plane displacement shapes are quasi-linear. Table 10 also gives the critical buckling loads of Al/Al_2O_3 square sandwich plates under biaxial compressions.

Example 6: Finally, Tables 11 and 12 contain the fundamental frequencies and critical buckling loads of Al/Al_2O_3 sandwich plates of Type C of present study along with those by SSDT, TSDT [47], HDT [49], quasi-3D ([45], [53]) and 3D [48]. They are carried out for six types of plates with different values of the power-law index. It can be seen that the present theory provides excellent solution for Type C plates. It implies that the proposed theory is appropriate and efficient for analyzing static, vibration and buckling responses of sandwich plates. Figure 6 shows the fundamental frequencies and critical buckling loads of sandwich plates with respect to the power-law index. It can be seen from this figure that they decrease with the increase of the power-law index. The lowest and highest values of natural frequency and critical buckling load correspond to the (1-0-1) and (1-2-1) sandwich plates, respectively. It is due to the fact that these plates correspond to the lowest and highest volume fractions of the ceramic phase, and thus makes them become the softest and hardest ones.

4. Conclusions

A new inverse trigonometric shear deformation theory has been proposed for the static bending, buckling and free vibration analyses of isotropic and FG sandwich plates. Three different types of FG plates are considered: FG plates, sandwich plates with FG core and sandwich plates with FG faces. Analytical solutions are obtained for simply-supported sandwich plates to investigate the deflections, stresses, critical buckling load and natural frequencies for various power-law index and side-to-thickness and skin-core-skin thickness ratios. A good agreement between the obtained results and those predicted by existing shear deformation theories is established through several numerical examples which demonstrates the accuracy of the present theory in predicting the bending, buckling and vibration responses of FG sandwich plates.

Acknowledgements

This research is funded by Vietnam National Foundation for Science and Technology Development (NAFOSTED) under Grant No. 107.02-2012.07.

References

References

[1] M. Koizumi, FGM Activities in Japan, Composites Part B: Engineering 28 (1997) 1–4.

[2] E. Feldman, J. Aboudi, Buckling analysis of functionally graded plates subjected to uniaxial loading, Composite Structures 38 (1997) 29–36.

[3] R. Javaheri, M. Eslami, Buckling of functionally graded plates under in-plane compressive loading, Journal of Applied Mathematics and Mechanics 82 (2002) 277–283.

[4] M. Mahdavian, Buckling analysis of simply-supported functionally graded rectangular plates under non-uniform in-plane compressive loading, Journal of Solid Mechanics 1 (2009) 213–225.

[5] M. Mohammadi, A. Saidi, E. Jomehzadeh, Levy solution for buckling analysis of functionally graded rectangular plates, Applied Composite Materials 17 (2010) 81–93.

[6] C. S. Chen, T. J. Chen, R. D. Chien, Nonlinear vibration of initially stressed functionally graded plates, Thin-Walled Structures 44 (8) (2006) 844–851.

[7] A. H. Baferani, A. R. Saidi, E. Jomehzadeh, An exact solution for free vibration of thin functionally graded rectangular plates, Proceedings of the Institution of Mechanical Engineers, Part C: Journal of Mechanical Engineering Science 225 (2011) 526–536.

[8] G. N. Praveen, J. N. Reddy, Nonlinear transient thermoelastic analysis of functionally graded ceramic-metal plates, International Journal of Solids and Structures 35 (1998) 4457–4476.

[9] L. D. Croce, P. Venini, Finite elements for functionally graded Reissner-Mindlin plates, Computer Methods in Applied Mechanics and Engineering 193 (2004) 705–725.

[10] E. Efraim, M. Eisenberger, Exact vibration analysis of variable thickness thick annular isotropic and FGM plates, Journal of Sound and Vibration 299 (2007) 720–738.

[11] X. Zhao, Y. Y. Lee, K. M. Liew, Mechanical and thermal buckling analysis of functionally graded plates, Composite Structures 90 (2009) 161–171.

[12] X. Zhao, Y. Y. Lee, K. M. Liew, Free vibration analysis of functionally graded plates using the element-free kp-Ritz method, Journal of Sound and Vibration 319 (2009) 918–939.

[13] S. Hosseini-Hashemi, M. Fadaee, S. R. Atashipour, A new exact analytical approach for free vibration of Reissner-Mindlin functionally graded rectangular plates, International Journal of Mechanical Sciences 53 (2011) 11–22.

[14] A. Naderi, A. Saidi, On pre-buckling configuration of functionally graded Mindlin rectangular plates, Mechanics Research Communications 37 (2010) 535–538.

[15] J. N. Reddy, Analysis of functionally graded plates, International Journal for Numerical Methods in Engineering 47 (2000) 663–684.

[16] H.-T. Thai, T. P. Vo. A new sinusoidal shear deformation theory for bending, buckling, and vibration of functionally graded plates Applied Mathematical Modelling 37 (2013) 3269 – 3281

[17] D. K. Jha, T. Kant, R. K. Singh, Free vibration response of functionally graded thick plates with shear and normal deformations effects, Composite Structures 96 (2013) 799–823.

[18] J. N. Reddy, A general nonlinear third-order theory of functionally graded plates, International Journal of Aerospace and Lightweight Structures 1 (2011) 1–21.

[19] M. Talha, B. N. Singh, Static response and free vibration analysis of FGM plates using higher order shear deformation theory, Applied Mathematical Modelling 34 (2010) 3991–4011.

[20] A. M. Zenkour, Generalized shear deformation theory for bending analysis of functionally graded materials, Applied Mathematical Modelling 30 (2006) 67–84.

[21] A. M. Zenkour, A simple four-unknown refined theory for bending analysis of functionally graded plates, Applied Mathematical Modelling 37 (20-21) (2013) 9041 – 9051.

[22] H. Matsunaga, Free vibration and stability of functionally graded plates according to a 2-D higher-order deformation theory, Composite Structures 82 (2008) 499–512.

[23] H.-T. Thai, S. E. Kim, A simple higher-order shear deformation theory for bending and free vibration analysis of functionally graded plates, Composite Structures 96 (2013) 165–173.

[24] H.-T. Thai, D. H. Choi, An efficient and simple refined theory for buckling analysis of functionally graded plates, Applied Mathematical Modelling 36 (2012) 1008–1022.

[25] J. L. Mantari, A. S. Oktem, O. G. Soares, Bending response of functionally graded plates by using a new higher order shear deformation theory, Composite Structures 94 (2012) 714–723.

[26] E. Carrera, S. Brischetto, A. Robaldo, Variable kinematic model for the analysis of functionally graded material plates, AIAA Journal 46 (1) (2008) 194 – 203.

[27] C.-P. Wu, K.-H. Chiu, RMVT-based meshless collocation and element-free Galerkin methods for the quasi-3D free vibration analysis of multilayered composite and FGM plates , Composite Structures 93 (5) (2011) 1433 – 1448.

[28] A. M. A. Neves, A. J. M. Ferreira, E. Carrera, M. Cinefra, C. M. C. Roque, R. M. N. Jorge, C. M. M. Soares, A quasi-3D hyperbolic shear deformation theory for the static and free vibration analysis of functionally graded plates, Composite Structures 94 (2012) 1814–1825.

[29] A. M. A. Neves, A. J. M. Ferreira, E. Carrera, C. M. C. Roque, M. Cinefra, R. M. N. Jorge, C. M. M. Soares, A quasi-3D sinusoidal shear deformation theory for the static and free vibration analysis of functionally graded plates, Composites Part B: Engineering 43 (2012) 711–725.

[30] J. L. Mantari, C. G. Soares, Generalized hybrid quasi-3D shear deformation theory for the static analysis of advanced composite plates, Composite Structures 94 (8) (2012) 2561 – 2575.

[31] J. L. Mantari, C. G. Soares, A novel higher-order shear deformation theory with stretching effect for functionally graded plates, Composites Part B: Engineering 45 (1) (2013) 268 – 281.

[32] C. Chen, C. Hsu, G. Tzou, Vibration and stability of functionally graded plates based on a higher-order deformation theory, Journal of Reinforced Plastics and Composites 28 (2009) 1215–1234.

[33] D. K. Jha, T. Kant, R. K. Singh, Free vibration response of functionally graded thick plates with shear and normal deformations effects, Composite Structures 96 (2013) 799–823.

[34] H.-T. Thai, S.-E. Kim, A simple quasi-3D sinusoidal shear deformation theory for functionally graded plates, Composite Structures 99 (2013) 172 – 180.

[35] H.-T. Thai, T. P. Vo, T. Bui, T.-K. Nguyen, A quasi-3D hyperbolic shear deformation theory for functionally graded plates, Acta Mechanica (2013) 1–14.

[36] A. Zenkour, Benchmark trigonometric and 3-d elasticity solutions for an exponentially graded thick rectangular plate, Archive of Applied Mechanics 77 (4) (2007) 197–214.

[37] B. Uymaz, M. Aydogdu, Three-dimensional vibration analyses of functionally graded plates under various boundary conditions, Journal of Reinforced Plastics and Composites 26 (18) (2007) 1847–1863.

[38] A. M. A. Neves, A. J. M. Ferreira, E. Carrera, M. Cinefra, C. M. C. Roque, R. M. N. Jorge, C. M. M. Soares, Static, free vibration and buckling analysis of isotropic and sandwich functionally graded plates using a quasi-3D higher-order shear deformation theory and a meshless technique, Composites Part B: Engineering 44 (2013) 657–674.

[39] A. M. Zenkour, A comprehensive analysis of functionally graded sandwich plates: Part 1 Deflection and stresses, International Journal of Solids and Structures 42 (2005) 5224–5242.

[40] S. Brischetto, Classical and mixed advanced models for sandwich plates embedding functionally graded cores, Journal of Mechanics of Materials and Structures 4 (2009) 13–33.

[41] A. Hamidi, M. Zidi, M. S. A. Houari, A. Tounsi, A new four variable refined plate theory for bending response of functionally graded sandwich plates under thermomechanical loading, Composites Part B: Engineering (0) (2012) In Press.

[42] H. H. Abdelaziz, H. A. Atmane, I. Mechab, L. Boumia, A. Tounsi, A. B. E. Abbas, Static analysis of functionally graded sandwich plates using an efficient and simple refined theory, Chinese Journal of Aeronautics 24 (4) (2011) 434 – 448.

[43] E. Carrera, S. Brischetto, M. Cinefra, M. Soave, Effects of thickness stretching in functionally graded plates and shells, Composites Part B: Engineering 42 (2) (2011) 123 – 133.

[44] A. M. Zenkour, Bending analysis of functionally graded sandwich plates using a simple four-unknown shear and normal deformations theory, Journal of Sandwich Structures and Materials 15 (2013) 629–656.

[45] A. Bessaim, M. S. Houari, A. Tounsi, S. Mahmoud, E. A. Adda Bedia, A new higher-order shear and normal deformation theory for the static and free vibration analysis of sandwich plates with functionally graded isotropic face sheets, Journal of Sandwich Structures and Materials 15 (2013) 671–703.

[46] H.-T. Thai, T.-K. Nguyen, T. P. Vo, J. Lee, Analysis of functionally graded sandwich plates using a new first-order shear deformation theory, European Journal of Mechanics - A/Solids 45 (2014) 211 – 225.

[47] A. M. Zenkour, A comprehensive analysis of functionally graded sandwich plates: Part 2 - Buckling and free vibration, International Journal of Solids and Structures 42 (2005) 5243–5258.

[48] Q. Li, V. P. Iu, K. P. Kou, Three-dimensional vibration analysis of functionally graded material sandwich plates, Journal of Sound and Vibration 311 (2008) 498–515.

[49] N. E. Meiche, A. Tounsi, N. Ziane, I. Mechab, E. A. Adda.Bedia, A new hyperbolic shear deformation theory for buckling and vibration of functionally graded sandwich plate, International Journal of Mechanical Sciences 53 (4) (2011) 237 – 247.

[50] M. Sobhy, Buckling and free vibration of exponentially graded sandwich plates resting on elastic foundations under various boundary conditions, Composite Structures 99 (2013) 76 – 87.

[51] T.-K. Nguyen, T. P. Vo, H.-T. Thai. Vibration and buckling analysis of functionally graded sandwich plates with improved transverse shear stiffness based on the first-order shear deformation

theory, Proceedings of the Institution of Mechanical Engineers, Part C: Journal of Mechanical Engineering Science, 2013, In Press.

[52] S. Natarajan, G. Manickam, Bending and vibration of functionally graded material sandwich plates using an accurate theory, Finite Elements in Analysis and Design 57 (2012) 32 – 42.

[53] A. Neves, A. Ferreira, E. Carrera, M. Cinefra, R. Jorge, C. Soares, Buckling analysis of sandwich plates with functionally graded skins using a new quasi-3D hyperbolic sine shear deformation theory and collocation with radial basis functions, Journal of Applied Mathematics and Mechanics 92 (2012) 749–766.

CAPTIONS OF TABLES

Table 1: Material properties of metal and ceramic.

Table 2: Comparison of the nondimensional stress and displacements of Al/Al_2O_3 square plates (a/h=10, Type A).

Table 3: Comparison of the nondimensional stress and displacements of Al/Al_2O_3 square sandwich plates (a/h=10, Type B).

Table 4: Nondimensional center deflections ($\hat{w}$) of Al/ZrO_2 square sandwich plates (a/h=10, Type C).

Table 5: Nondimensional axial stress ($\hat{\sigma}_{xx}$(h/2)) of Al/ZrO_2 square sandwich plates (a/h=10, Type C).

Table 6: Nondimensional shear stress ($\bar{\sigma}_{xz}(0)$) of Al/ZrO_2 square sandwich plates (a/h=10, Type C).

Table 7: Comparison of the nondimensional fundamental frequency ($\bar{\omega}$) of Al^*/ZrO_2 square plates (Type A).

Table 8: Comparison of the critical buckling load ($\bar{N}_{cr}$) of Al/Al_2O_3 plates (Type A).

Table 9: Comparison of the nondimensional fundamental frequency ($\hat{\omega}$) of Al/Al_2O_3 square sandwich plates (Type B).

Table 10: Nondimensional critical buckling loads ($\hat{N}_{cr}$) of Al/Al_2O_3 square sandwich plates subjected to biaxial compressive loads ($\gamma = 1$, Type B).

Table 11: Nondimensional fundamental frequency ($\hat{\omega}$) of Al/Al_2O_3 square sandwich plates (a/h=10, Type C).

Table 12: Nondimensional critical buckling loads ($\hat{N}_{cr}$) of Al/Al_2O_3 square sandwich plates subjected to biaxial compressive loads ($\gamma = 1$, a/h=10, Type C).

CAPTIONS OF FIGURES

Figure 1: Geometry of functionally graded plates.

Figure 2: 1-2-1 sandwich plates for several power-law index (p).

Figure 3: Estimation of the parameter r for analysis of isotropic and functionally graded sandwich plates (a/h=10).

Figure 4: Nondimensional stresses through the thickness direction for different values of p of Al/Al_2O_3 square plates subjected to sinusoidal load (a/h=10, Type A).

Figure 5: Nondimensional stresses through the thickness direction for different values of p of Al/Al_2O_3 and Al/ZrO_2 square sandwich plates subjected to sinusoidal load with (a/h=10, Type B and Type C).

Figure 6: Effect of the power-law index p on the nondimensional fundamental frequency ($\hat{\omega}$) and critical buckling load ($\hat{N}_{cr}$) of Al/Al_2O_3 square sandwich plates (a/h=10, Type C).

Figure 7: Displacement shapes of six modes of (1-2-1) Al/Al_2O_3 square sandwich plates (a/h=10, p=5, x=a/4, y=b/4, Type B).

Table 1: Material properties of metal and ceramic

Material	Young's modulus (GPa)	Mass density (kg/m^3)	Poisson's ratio
Aluminum (Al^*)	70	2702	0.3
Aluminum (Al)	70	2707	0.3
Zirconia (ZrO_2)	151	3000	0.3
Alumina (Al_2O_3)	380	3800	0.3

Table 2: Comparison of the nondimensional stress and displacements of Al/Al_2O_3 square plates (a/h=10, Type A).

p	Theory	$\bar{u}(-h/4)$	$\bar{w}$	$\bar{\sigma}_{xx}(h/3)$	$\bar{\sigma}_{xy}(-h/3)$	$\bar{\sigma}_{xz}(h/6)$
1	Present	0.6413	0.5890	1.4897	0.6111	0.2611
	Quasi-3D [26]	0.6436	0.5875	1.5062	0.6081	0.2510
	Quasi-3D [27]	0.6436	0.5876	1.5061	0.6112	0.2511
	SSDT [20]	0.6626	0.5889	1.4894	0.6110	0.2622
	HSDT [25]	0.6398	0.5880	1.4888	0.6109	0.2566
	TSDT [23]	0.6414	0.5890	1.4898	0.6111	0.2608
2	Present	0.8982	0.7573	1.3959	0.5442	0.2742
	Quasi-3D [26]	0.9012	0.7570	1.4147	0.5421	0.2496
	Quasi-3D [27]	0.9013	0.7571	1.4133	0.5436	0.2495
	SSDT [20]	0.9281	0.7573	1.3954	0.5441	0.2763
	HSDT [25]	0.8957	0.7564	1.3940	0.5438	0.2741
	TSDT [23]	0.8984	0.7573	1.3960	0.5442	0.2737
4	Present	1.0500	0.8816	1.1792	0.5669	0.2546
	Quasi-3D [26]	1.0541	0.8823	1.1985	0.5666	0.2362
	Quasi-3D [27]	1.0541	0.8823	1.1841	0.5671	0.2362
	SSDT [20]	1.0941	0.8819	1.1783	0.5667	0.2580
	HSDT [25]	1.0457	0.8814	1.1755	0.5662	0.2623
	TSDT [23]	1.0502	0.8815	1.1794	0.5669	0.2537
8	Present	1.0759	0.9746	0.9473	0.5857	0.2094
	Quasi-3D [26]	1.0830	0.9738	0.9687	0.5879	0.2262
	Quasi-3D [27]	1.0830	0.9739	0.9622	0.5883	0.2261
	SSDT [20]	1.1340	0.9750	0.9466	0.5856	0.2121
	HSDT [25]	1.0709	0.9737	0.9431	0.5850	0.2140
	TSDT [23]	1.0763	0.9746	0.9477	0.5858	0.2088

Table 3: Comparison of the nondimensional stress and displacements of Al/Al_2O_3 square sandwich plates (a/h=10, Type B).

p	Theory	$\bar{u}(-h/4)$	$\bar{w}$	$\bar{\sigma}_{xx}(h/3)$	$\bar{\sigma}_{xy}(-h/3)$	$\bar{\sigma}_{xz}(h/6)$
0	Present	0.3247	0.3744	1.4761	1.0130	0.2161
	Quasi-3D [38]	-	0.3711	-	-	0.2227
0.5	Present	0.5542	0.5245	1.5750	0.6965	0.2509
	Quasi-3D [38]	-	0.5238	-	-	0.2581
1	Present	0.7337	0.6345	1.5691	0.5447	0.2733
	FSDT [40]	-	0.6337	-	-	0.2458
	Quasi-3D [43]	-	0.6324	-	-	0.2594
	Quasi-3D [29]	-	0.6305	-	-	0.2788
	Quasi-3D [38]	-	0.6305	-	-	0.2789
4	Present	1.0550	0.8331	1.2539	0.5614	0.2697
	FSDT [40]	-	0.8191	-	-	0.1877
	Quasi-3D [43]	-	0.8307	-	-	0.2398
	Quasi-3D [29]	-	0.8202	-	-	0.2778
	Quasi-3D [38]	-	0.8199	-	-	0.2747
10	Present	1.0798	0.8807	0.9258	0.5758	0.1982
	FSDT [40]	-	0.8556	-	-	0.1234
	Quasi-3D [43]	-	0.8740	-	-	0.1944
	Quasi-3D [29]	-	0.8650	-	-	0.2059
	Quasi-3D [38]	-	0.8645	-	-	0.2034

Table 4: Nondimensional center deflections ($\hat{w}$) of Al/ZrO_2 square sandwich plates (a/h=10, Type C).

p	Theory	1-0-1	2-1-2	2-1-1	1-1-1	2-2-1	1-2-1
0	Present	0.19597	0.19597	0.19597	0.19597	0.19597	0.19597
	Zenkour [39] (TSDT)	0.19606	0.19606	-	0.19606	0.19606	0.19606
	Zenkour [39] (SSDT)	0.19605	0.19605	-	0.19605	0.19605	0.19605
	Zenkour [44] (Quasi-3D)	0.19487	0.19487	-	0.19487	0.19487	0.19487
	Neves et al. [38] (Quasi-3D)	-	0.19490	0.19490	0.19490	0.19490	0.19490
	Bessaim et al. [45] (Quasi-3D)	-	0.19486	0.19486	0.19486	0.19486	0.19486
1	Present	0.32348	0.30622	0.29666	0.29191	0.28077	0.27086
	Zenkour [39] (TSDT)	0.32358	0.30632	-	0.29199	0.28085	0.27094
	Zenkour [39] (SSDT)	0.32349	0.30624	-	0.29194	0.28082	0.27093
	Zenkour [44] (Quasi-3D)	0.32001	0.30275	-	0.28867	0.27760	0.26815
	Neves et al. [38] (Quasi-3D)	-	0.30700	0.29750	0.29290	0.28200	0.27220
	Bessaim et al. [45] (Quasi-3D)	-	0.30430	0.29448	0.29007	0.27874	0.26915
2	Present	0.37322	0.35221	0.33769	0.33279	0.31608	0.30255
	Zenkour [39] (TSDT)	0.37335	0.35231	-	0.33289	0.31617	0.30263
	Zenkour [39] (SSDT)	0.37319	0.35218	-	0.33280	0.31611	0.30260
	Zenkour [44] (Quasi-3D)	0.36891	0.34737	-	0.32816	0.31152	0.29874
	Neves et al. [38] (Quasi-3D)	-	0.35190	0.33760	0.33290	0.31640	0.30320
	Bessaim et al. [45] (Quasi-3D)	-	0.35001	0.33495	0.33068	0.31356	0.30060
5	Present	0.40911	0.39170	0.37295	0.37134	0.34950	0.33472
	Zenkour [39] (TSDT)	0.40927	0.39183	-	0.37145	0.34960	0.33480
	Zenkour [39] (SSDT)	0.40905	0.39160	-	0.37128	0.34950	0.33474
	Zenkour [44] (Quasi-3D)	0.40532	0.38612	-	0.36546	0.34361	0.32966
	Neves et al. [38] (Quasi-3D)	-	0.39050	0.37220	0.37050	0.34900	0.33470
	Bessaim et al. [45] (Quasi-3D)	-	0.38934	0.36981	0.36902	0.34649	0.33255
10	Present	0.41754	0.40393	0.3843	0.38540	0.36202	0.34815
	Zenkour [39] (TSDT)	0.41772	0.40407	-	0.38551	0.36215	0.34824
	Zenkour [39] (SSDT)	0.41750	0.40376	-	0.38490	0.34916	0.34119
	Zenkour [44] (Quasi-3D)	0.41448	0.39856	-	0.37924	0.35577	0.34259
	Neves et al. [38] (Quasi-3D)	-	0.40260	0.38350	0.38430	0.36120	0.34800
	Bessaim et al. [45] (Quasi-3D)	-	0.40153	0.38111	0.38303	0.35885	0.34591

Table 5: Nondimensional axial stress ($\hat{\sigma}_{xx}$(h/2)) of Al/ZrO_2 square sandwich plates (a/h=10, Type C).

p	Theory	1-0-1	2-1-2	2-1-1	1-1-1	2-2-1	1-2-1
0	Present	1.99482	1.99482	1.99482	1.99482	1.99482	1.99482
	Zenkour [39] (TSDT)	2.04985	2.04985	-	2.04985	2.04985	2.04985
	Zenkour [39] (SSDT)	2.05452	2.05452	-	2.05452	2.05452	2.05452
	Zenkour [44] (Quasi-3D)	2.00773	2.00773	-	2.00773	2.00773	2.00773
	Neves et al. [38] (Quasi-3D)	-	2.00660	2.00640	2.00660	2.00650	2.00640
	Bessaim et al. [45] (Quasi-3D)	-	1.99524	1.99524	1.99524	1.99524	1.99524
1.0	Present	1.54441	1.46297	1.35703	1.39406	1.28852	1.29174
	Zenkour [39] (TSDT)	1.57923	1.49587	-	1.42617	1.32062	1.32309
	Zenkour [39] (SSDT)	1.58204	1.49859	-	1.42892	1.32342	1.32590
	Zenkour [44] (Quasi-3D)	1.57004	1.48833	-	1.41781	1.30907	1.31204
	Neves et al. [38] (Quasi-3D)	-	1.48130	1.37680	1.41370	1.30920	1.31330
	Bessaim et al. [45] (Quasi-3D)	-	1.46131	1.35053	1.39243	1.28274	1.29030
2.0	Present	1.78383	1.68682	1.52988	1.59393	1.43693	1.44707
	Zenkour [39] (TSDT)	1.82167	1.72144	-	1.62748	1.47095	1.47988
	Zenkour [39] (SSDT)	1.82450	1.72412	-	1.63025	1.47387	1.48283
	Zenkour [44] (Quasi-3D)	1.81509	1.72030	-	1.62591	1.46372	1.47421
	Neves et al. [38] (Quasi-3D)	-	1.69940	1.54560	1.60880	1.45430	1.46590
	Bessaim et al. [45] (Quasi-3D)	-	1.68472	1.52101	1.59170	1.42887	1.44497
5.0	Present	1.95031	1.87709	1.67895	1.78159	1.57620	1.60459
	Zenkour [39] (TSDT)	1.99272	1.91302	-	1.81580	1.61181	1.63814
	Zenkour [39] (SSDT)	1.99567	1.91547	-	1.81838	1.61477	1.64106
	Zenkour [44] (Quasi-3D)	1.97912	1.91504	-	1.82018	1.60953	1.63906
	Neves et al. [38] (Quasi-3D)	-	1.88380	1.69090	1.79060	1.58930	1.61950
	Bessaim et al. [45] (Quasi-3D)	-	1.87516	1.66856	1.77919	1.56627	1.60203
10.0	Present	1.98382	1.93431	1.72890	1.84933	1.62840	1.67019
	Zenkour [39] (TSDT)	2.03036	1.97126	-	1.88376	1.66660	1.70417
	Zenkour [39] (SSDT)	2.03360	1.97313	-	1.88147	1.61979	1.64851
	Zenkour [44] (Quasi-3D)	2.00692	1.97075	-	1.89162	2.18558	1.67350
	Neves et al. [38] (Quasi-3D)	-	1.93970	1.74050	1.85590	1.63950	1.68320
	Bessaim et al. [45] (Quasi-3D)	-	1.93266	1.71835	1.84705	1.61792	1.66754

Table 6: Nondimensional shear stress ($\bar{\sigma}_{xz}(0)$) of Al/ZrO_2 square sandwich plates (a/h=10, Type C).

p	Theory	1-0-1	2-1-2	2-1-1	1-1-1	2-2-1	1-2-1
0	Present	0.23581	0.23581	0.23581	0.23581	0.23581	0.23581
	Zenkour [39] (TSDT)	0.23857	0.23857	-	0.23857	0.23857	0.23857
	Zenkour [39] (SSDT)	0.24618	0.24618	-	0.24618	0.24618	0.24618
	Zenkour [44] (Quasi-3D)	0.23910	0.23910	-	0.23910	0.23910	0.23910
	Neves et al. [38] (Quasi-3D)	-	0.25380	0.22910	0.24610	0.24110	0.23630
	Bessaim et al. [45] (Quasi-3D)	-	0.23794	0.23794	0.23794	0.23794	0.23794
1.0	Present	0.28953	0.26882	0.26852	0.25906	0.25736	0.25054
	Zenkour [39] (TSDT)	0.29203	0.27104	-	0.26117	0.25951	0.25258
	Zenkour [39] (SSDT)	0.29907	0.27774	-	0.26809	0.26680	0.26004
	Zenkour [44] (Quasi-3D)	0.36531	0.34366	-	0.32853	0.31785	0.30845
	Neves et al. [38] (Quasi-3D)	-	0.27450	0.26400	0.26430	0.25940	0.24960
	Bessaim et al. [45] (Quasi-3D)	-	0.27050	0.27017	0.26060	0.25890	0.25196
2.0	Present	0.32336	0.28607	0.28569	0.26982	0.26731	0.25645
	Zenkour [39] (TSDT)	0.32622	0.28838	-	0.27188	0.26939	0.25834
	Zenkour [39] (SSDT)	0.33285	0.29422	-	0.27807	0.27627	0.26543
	Zenkour [44] (Quasi-3D)	0.41778	0.38601	-	0.36417	0.34824	0.33543
	Neves et al. [38] (Quasi-3D)	-	0.27600	0.28770	0.26680	0.26360	0.25230
	Bessaim et al. [45] (Quasi-3D)	-	0.28792	0.28742	0.27138	0.26885	0.25776
5.0	Present	0.38250	0.31182	0.31087	0.28420	0.28047	0.26327
	Zenkour [39] (TSDT)	0.38634	0.31454	-	0.28643	0.28265	0.26512
	Zenkour [39] (SSDT)	0.39370	0.31930	-	0.29150	0.28895	0.27153
	Zenkour [44] (Quasi-3D)	0.46890	0.42723	-	0.39918	0.37791	0.36234
	Neves et al. [38] (Quasi-3D)	-	0.27120	0.33770	0.26550	0.26690	0.25460
	Bessaim et al. [45] (Quasi-3D)	-	0.31419	0.31293	0.28606	0.28217	0.26463
10.0	Present	0.42744	0.32936	0.32732	0.29326	0.28854	0.26705
	Zenkour [39] (TSDT)	0.43206	0.33242	-	0.29566	0.29080	0.26895
	Zenkour [39] (SSDT)	0.44147	0.33644	-	0.29529	0.29671	0.27676
	Zenkour [44] (Quasi-3D)	0.49051	0.44435	-	0.41385	0.39045	0.37390
	Neves et al. [38] (Quasi-3D)	-	0.26710	0.38060	0.26390	0.26920	0.25680
	Bessaim et al. [45] (Quasi-3D)	-	0.33210	0.32959	0.29534	0.29036	0.26850

Table 7: Comparison of the nondimensional fundamental frequency ($\bar{\omega}$) of Al^*/ZrO_2 square plates (Type A).

a/h	Theory	Power-law index							
		0	0.1	0.2	0.5	1	2	5	10
2	Present	1.2454	1.2162	1.1913	1.1356	1.0784	1.0234	0.9685	0.9435
	3D [37]	1.2589	1.2296	1.2049	1.1484	1.0913	1.0344	0.9777	0.9507
5	Present	1.7683	1.7208	1.6818	1.5974	1.5212	1.4601	1.4058	1.3690
	3D [37]	1.7748	1.7262	1.6881	1.6031	1.4764	1.4628	1.4106	1.3711
10	Present	1.9317	1.8773	1.8332	1.7393	1.6583	1.5986	1.5492	1.5083
	3D [37]	1.9339	1.8788	1.8357	1.7406	1.6583	1.5968	1.5491	1.5066
20	Present	1.9821	1.9254	1.8797	1.7827	1.7003	1.6415	1.5943	1.5521
	3D [37]	1.9570	1.9261	1.8788	1.7832	1.6999	1.6401	1.5937	1.5491
50	Present	1.9971	1.9397	1.8935	1.7956	1.7129	1.6543	1.6078	1.5652
	3D [37]	1.9974	1.9390	1.8920	1.7944	1.7117	1.6522	1.6062	1.5620
100	Present	1.9993	1.9418	1.8955	1.7975	1.7147	1.6562	1.6098	1.5671
	3D [37]	1.9974	1.9416	1.8920	1.7972	1.7117	1.6552	1.6062	1.5652

Table 8: Comparison of the critical buckling load ($\bar{N}_{cr}$) of Al/Al_2O_3 plates (Type A).

γ	a/b	a/h	Theory	Power-law index p					
				0	0.5	1	2	5	10
0	0.5	5	Present	6.7204	4.4221	3.4164	2.6450	2.1479	1.9210
			TSDT [24]	6.7203	4.4235	3.4164	2.6451	2.1484	1.9213
		10	Present	7.4053	4.8190	3.7111	2.8896	2.4163	2.1897
			TSDT [24]	7.4053	4.8206	3.7111	2.8897	2.4165	2.1896
		20	Present	7.5993	4.9298	3.7930	2.9581	2.4944	2.2692
			TSDT [24]	7.5993	4.9315	3.7930	2.9582	2.4944	2.2690
	1	5	Present	16.0216	10.6215	8.2247	6.3430	5.0513	4.4800
			TSDT [24]	16.0211	10.6254	8.2245	6.3432	5.0531	4.4807
		10	Present	18.5786	12.1181	9.3391	7.2630	6.0346	5.4530
			TSDT [24]	18.5785	12.1229	9.3391	7.2631	6.0353	5.4528
		20	Present	19.3528	12.5616	9.6675	7.5371	6.3446	5.7674
			TSDT [24]	19.3528	12.5668	9.6675	7.5371	6.3448	5.7668
1	0.5	5	Present	5.3763	3.5377	2.7331	2.1160	1.7183	1.5368
			TSDT [24]	5.3762	3.5388	2.7331	2.1161	1.7187	1.5370
		10	Present	5.9243	3.8552	2.9689	2.3117	1.9330	1.7517
			TSDT [24]	5.9243	3.8565	2.9689	2.3117	1.9332	1.7517
		20	Present	6.0794	3.9438	3.0344	2.3665	1.9955	1.8153
			TSDT [24]	6.0794	3.9452	3.0344	2.3665	1.9955	1.8152
	1	5	Present	8.0108	5.3108	4.1124	3.1715	2.5256	2.2400
			TSDT [24]	8.0105	5.3127	4.1122	3.1716	2.5265	2.2403
		10	Present	9.2893	6.0590	4.6696	3.6315	3.0173	2.7265
			TSDT [24]	9.2893	6.0615	4.6696	3.6315	3.0177	2.7264
		20	Present	9.6764	6.2808	4.8337	3.7686	3.1723	2.8837
			TSDT [24]	9.6764	6.2834	4.8337	3.7686	3.1724	2.8834

Table 9: Comparison of the nondimensional fundamental frequency ($\hat{\omega}$) of Al/Al_2O_3 square sandwich plates (Type B).

a/h	Theory	1-1-1				1-2-1			2-2-1		
		0	0.5	1	5	0.5	1	5	0.5	1	5
5	Present	1.1147	1.1414	1.1561	1.1996	1.1574	1.1827	1.2569	1.1916	1.2268	1.3160
	HSDT9 [52]	1.1021	1.1449	1.1639	1.2113	1.1597	1.1884	1.2644	1.1965	1.2350	1.3249
	HSDT13 [52]	1.0893	1.1511	1.1701	1.2162	1.1663	1.1952	1.2712	1.2031	1.2421	1.3312
10	Present	1.2172	1.2359	1.2478	1.2883	1.2567	1.2763	1.3466	1.2827	1.3187	1.4130
	HSDT9 [52]	1.2138	1.2373	1.2506	1.2921	1.2578	1.2785	1.3492	1.2846	1.3216	1.4161
	HSDT13 [52]	1.2087	1.2392	1.2524	1.2935	1.2598	1.2806	1.3513	1.2865	1.3238	1.4180
100	Present	1.2617	1.2752	1.2853	1.3238	1.2984	1.3147	1.3824	1.3198	1.3558	1.4518
	HSDT9 [52]	1.2617	1.2751	1.2854	1.3239	1.2981	1.3148	1.3825	1.3198	1.3559	1.4519
	HSDT13 [52]	1.2616	1.2751	1.2854	1.3239	1.2981	1.3148	1.3825	1.3198	1.3559	1.4519

Table 10: Nondimensional critical buckling loads ($\hat{N}_{cr}$) of Al/Al_2O_3 square sandwich plates subjected to biaxial compressive loads ($\gamma = 1$, Type B).

a/h	Scheme	p				
		0	0.5	1	5	10
5	1-1-1	2.0513	2.2342	2.3333	2.5978	2.6834
	1-2-1	1.9456	2.2725	2.4387	2.8964	3.0545
	2-2-1	2.1369	2.5023	2.7056	3.2351	3.4009
10	1-1-1	2.3508	2.5165	2.6123	2.8848	2.9773
	1-2-1	2.3095	2.5768	2.7322	3.2063	3.3816
	2-2-1	2.3928	2.7898	3.0116	3.6028	3.7937
100	1-1-1	2.4773	2.6308	2.7236	2.9969	3.0918
	1-2-1	2.4730	2.7015	2.8495	3.3268	3.5087
	2-2-1	2.4963	2.9038	3.1320	3.7467	3.9476

Table 11: Nondimensional fundamental frequency ($\hat{\omega}$) of Al/Al_2O_3 square sandwich plates (a/h=10, Type C).

p	Theory	1-0-1	2-1-2	2-1-1	1-1-1	2-2-1	1-2-1
0	Present	1.82489	1.82489	1.82489	1.82489	1.82489	1.82489
	Zenkour [47] (TSDT)	1.82445	1.82445	1.82445	1.82445	1.82445	1.82445
	Zenkour [47] (SSDT)	1.82452	1.82452	1.82452	1.82452	1.82452	1.82452
	Meiche et al. [49] (HDT)	1.82449	1.82449	1.82449	1.82449	1.82449	1.82449
	Bessaim et al. [45] (Quasi-3D)	1.82682	1.82682	-	1.82682	1.82682	1.82682
	Li et al. [48] (3D)	1.82682	1.82682	-	1.82682	1.82682	1.82682
0.5	Present	1.44348	1.48355	1.50597	1.51885	1.54680	1.57437
	Zenkour [47] (TSDT)	1.44424	1.48408	1.51253	1.51922	1.55199	1.57451
	Zenkour [47] (SSDT)	1.44436	1.48418	1.51258	1.51927	1.55202	1.57450
	Meiche et al. [49] (HDT)	1.44419	1.48405	1.50636	1.51922	1.54714	1.57458
	Bessaim et al. [45] (Quasi-3D)	1.44621	1.48611	-	1.52130	1.55016	1.57670
	Li et al. [48] (3D)	1.44614	1.48608	-	1.52131	1.54926	1.57668
1.0	Present	1.24332	1.30024	1.33352	1.35345	1.39579	1.43948
	Zenkour [47] (TSDT)	1.24320	1.30011	1.34888	1.35333	1.40789	1.43934
	Zenkour [47] (SSDT)	1.24335	1.30023	1.34894	1.35339	1.40792	1.43931
	Meiche et al. [49] (HDT)	1.24310	1.30004	1.33328	1.35331	1.39559	1.43940
	Bessaim et al. [45] (Quasi-3D)	1.24495	1.30195	-	1.35527	1.39987	1.44143
	Li et al . [48] (3D)	1.24470	1.30181	-	1.35523	1.39763	1.44137
5.0	Present	0.94611	0.98193	1.03067	1.04473	1.10905	1.17403
	Zenkour [47] (TSDT)	0.94598	0.98184	1.07432	1.04466	1.14731	1.17397
	Zenkour [47] (SSDT)	0.94630	0.98207	1.07445	1.04481	1.14741	1.17399
	Meiche et al. [49] (HDT)	0.94574	0.98166	1.03033	1.04455	1.10875	1.17397
	Bessaim et al. [45] (Quasi-3D)	0.94716	0.98311	-	1.04613	1.11723	1.17579
	Li et al. [48] (3D)	0.94476	0.98103	-	1.04532	1.10983	1.17567
10.0	Present	0.92854	0.94305	0.99219	0.99558	1.06114	1.12320
	Zenkour [47] (TSDT)	0.92839	0.94297	1.03862	0.99551	1.10533	1.12314
	Zenkour [47] (SSDT)	0.92875	0.94332	1.04558	0.99519	1.04154	1.13460
	Meiche et al. [49] (HDT)	0.92811	0.94275	0.99184	0.99536	1.06081	1.12311
	Bessaim et al. [45] (Quasi-3D)	0.92952	0.94410	-	0.99684	1.07015	1.12486
	Li et al. [48] (3D)	0.92727	0.94078	-	0.99523	1.06104	1.12466

Table 12: Nondimensional critical buckling loads ($\hat{N}_{cr}$) of Al/Al_2O_3 square sandwich plates subjected to biaxial compressive loads ($\gamma = 1$, a/h=10, Type C).

p	Theory	1-0-1	2-1-2	2-1-1	1-1-1	2-2-1	1-2-1
0	Present	6.50566	6.50566	6.50566	6.50566	6.50566	6.50566
	Zenkour [47] (TSDT)	6.50248	6.50248	6.50248	6.50248	6.50248	6.50248
	Zenkour [47] (SSDT)	6.50303	6.50303	6.50303	6.50303	6.50303	6.50303
	Meiche et al. [49] (HDT)	6.50276	6.50276	6.50276	6.50276	6.50276	6.50276
	Neves et al. [53] (HSDT)	6.50266	6.50266	6.50266	6.50266	6.50266	6.50266
	Neves et al. [53] (Quasi-3D)	6.47652	6.47652	6.47652	6.47652	6.47652	6.47652
0.5	Present	3.67832	3.96760	4.10999	4.21622	4.40304	4.60760
	Zenkour [47] (TSDT)	3.68219	3.97042	4.11235	4.21823	4.40499	4.60841
	Zenkour [47] (SSDT)	3.68284	3.97097	4.11269	4.21856	4.40519	4.60835
	Meiche et al. [49] (HDT)	3.68190	3.97023	4.11236	4.21823	4.40514	4.60878
	Neves et al. [53] (HSDT)	3.59354	3.87157	4.00853	4.11071	4.29073	4.48676
	Neves et al. [53] (Quasi-3D)	3.58096	3.85809	3.99480	4.09641	4.27592	4.47110
1	Present	2.58410	2.92060	3.09759	3.23299	3.47544	3.75403
	Zenkour [47] (TSDT)	2.58357	2.92003	3.09697	3.23237	3.47472	3.75328
	Zenkour [47] (SSDT)	2.58423	2.92060	3.09731	3.23270	3.47490	3.75314
	Meiche et al. [49] (SSDT)	2.58315	2.91970	3.09686	3.23225	3.47476	3.75359
	Neves et al. [53] (HSDT)	2.53913	2.86503	3.03679	3.16779	3.40280	3.67204
	Neves et al. [53] (Quasi-3D)	2.53062	2.85563	3.02733	3.15750	3.39207	3.66013
5	Present	1.32948	1.52155	1.70203	1.79002	2.05633	2.36760
	Zenkour [47] (TSDT)	1.32910	1.52129	1.70176	1.78978	2.05605	2.36734
	Zenkour [47] (SSDT)	1.33003	1.52203	1.70224	1.79032	2.05644	2.36744
	Meiche et al. [49] (HDT)	1.32839	1.52071	1.70140	1.78937	2.05578	2.36731
	Neves et al. [53] (HSDT)	1.32331	1.50935	1.68594	1.77072	2.03078	2.33036
	Neves et al. [53] (Quasi-3D)	1.31829	1.50409	1.68128	1.76507	2.02534	2.32354
10	Present	1.24406	1.37341	1.54622	1.59758	1.85403	2.14020
	Zenkour [47] (TSDT)	1.24363	1.37316	1.54595	1.59736	1.85376	2.13995
	Zenkour [47] (SSDT)	1.24475	1.37422	1.56721	1.59728	1.57287	2.19087
	Meiche et al. [49] (HDT)	1.24287	1.37249	1.54556	1.59687	1.85343	2.13982
	Neves et al. [53] (HSDT)	1.24090	1.36547	1.53468	1.58421	1.83573	2.10897
	Neves et al. [53] (Quasi-3D)	1.23599	1.36044	1.53036	1.57893	1.83083	2.10275

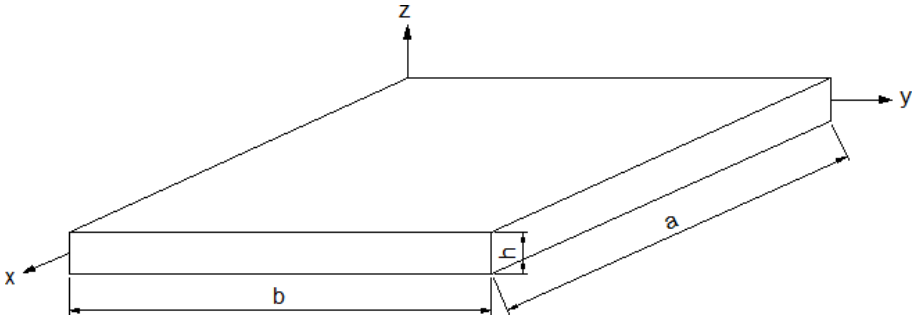

(a)

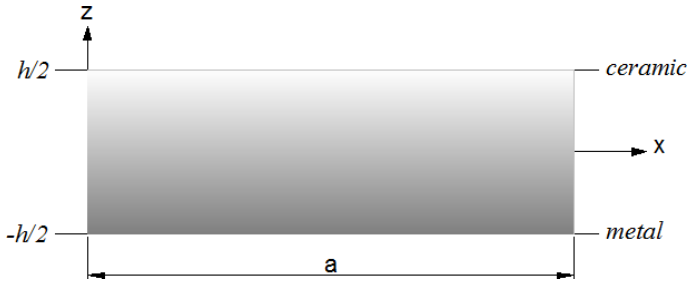

(b) Type A

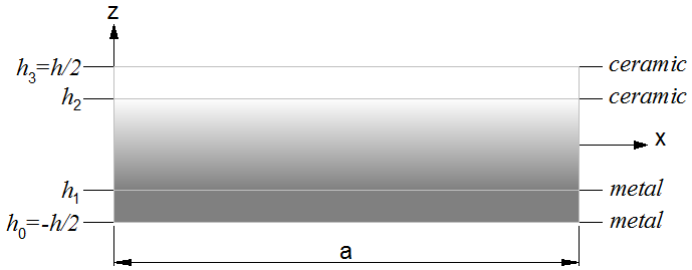

(c) Type B

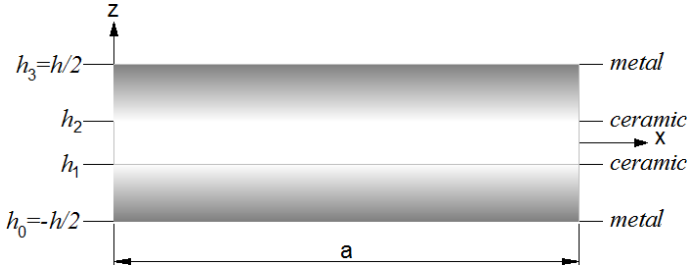

(d) Type C

Figure 1: Geometry of functionally graded plates.

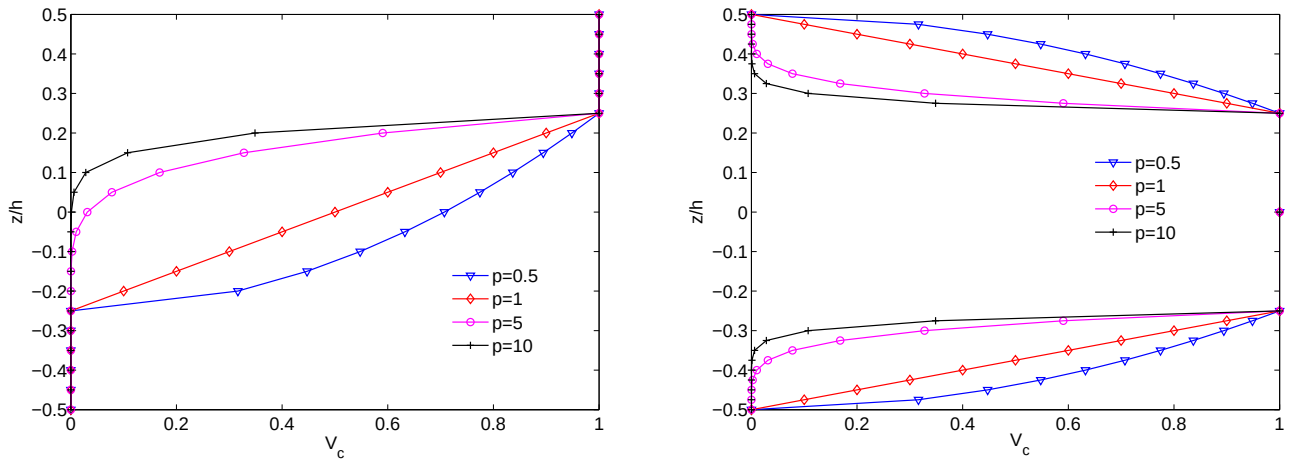

(a) Type B

(b) Type C

Figure 2: 1-2-1 sandwich plates for several power-law index (p).

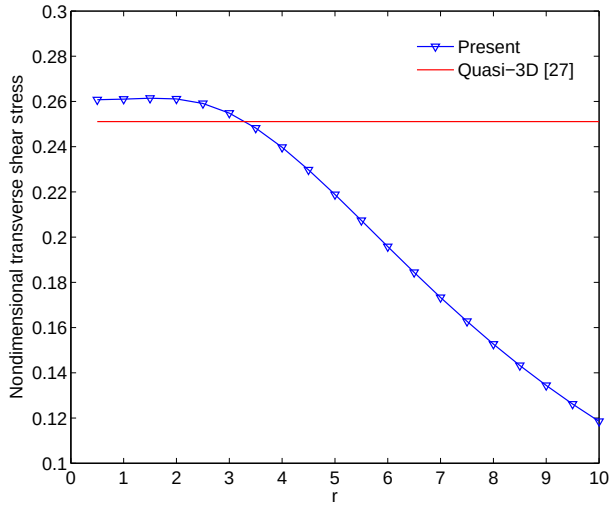

(a) Variation of $\bar{\sigma}_{xz}(h/6)$ with respect to r of Al/Al_2O_3 square plate (Type A) with p=1

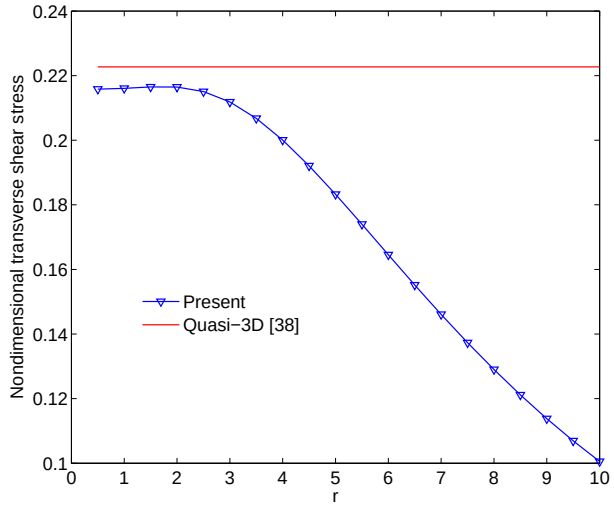

(b) Variation of $\bar{\sigma}_{xz}(h/6)$ with respect to r of (1-8-1) Al/Al_2O_3 square plate (Type B) with p=0

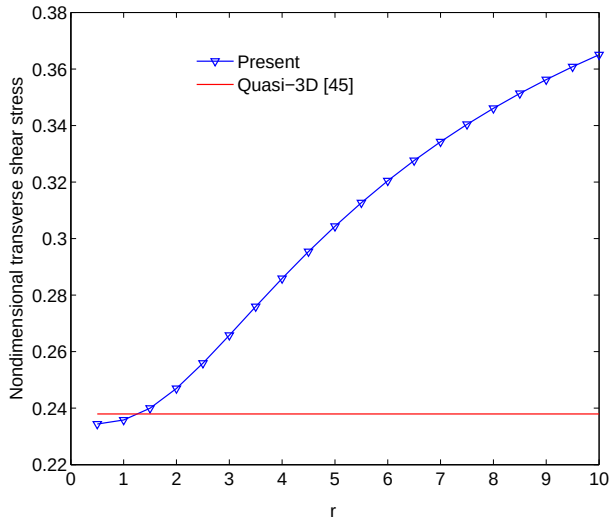

(c) Variation of $\bar{\sigma}_{xz}(0)$ with respect to r of (2-1-2) Al/ZrO_2 square plate (Type C) with p=0

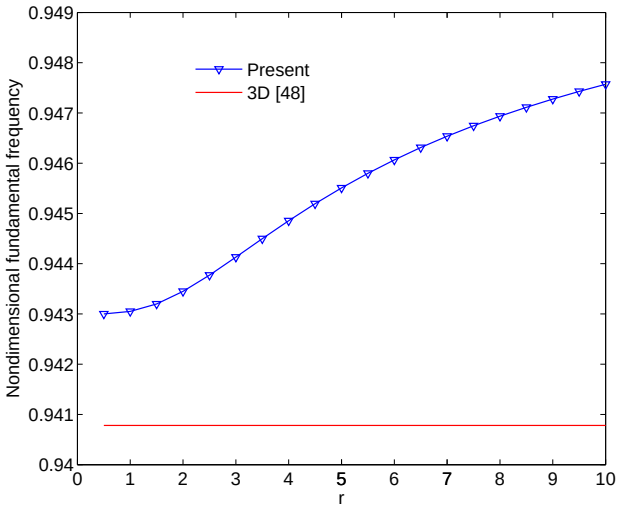

(d) Variation of $\hat{\omega}$ of (2-1-2) Al/Al_2O_3 square plate (Type C) with p=10

Figure 3: Estimation of the parameter r for analysis of isotropic and FG sandwich plates (a/h=10).

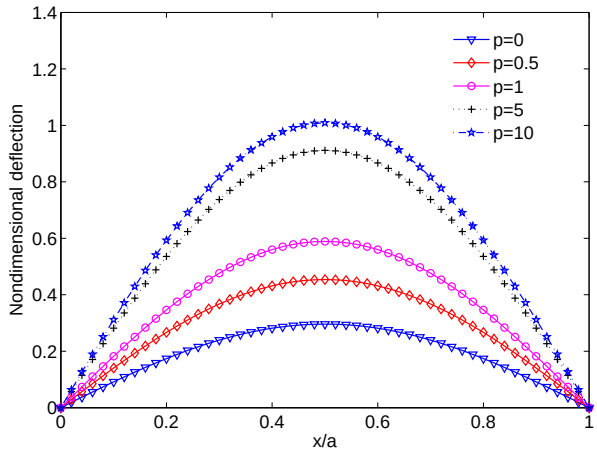

(a) $\bar{w}$

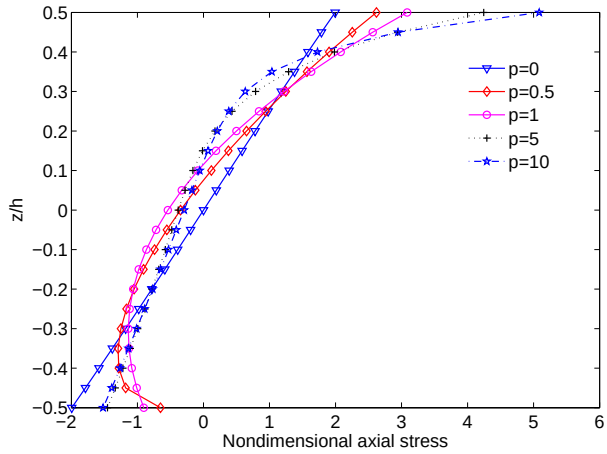

(b) $\bar{\sigma}_{xx}$

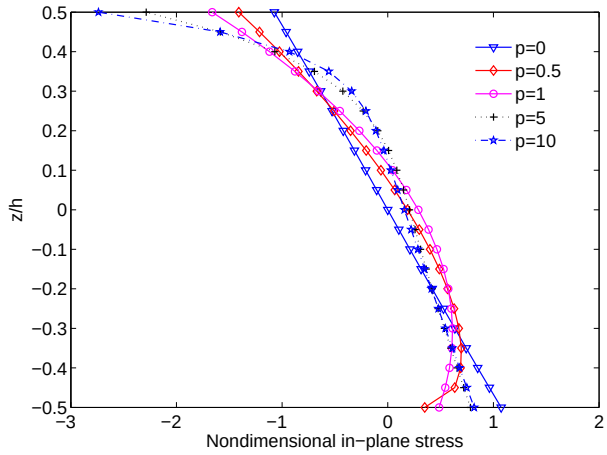

(c) $\bar{\sigma}_{xy}$

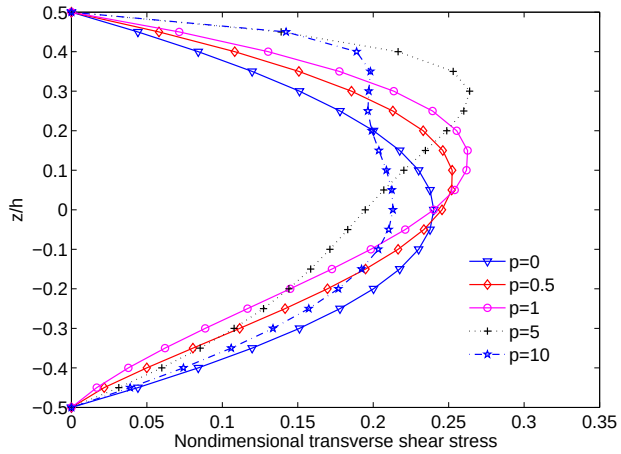

(d) $\bar{\sigma}_{xz}$

Figure 4: Nondimensional stresses through the thickness direction for different values of p of Al/Al_2O_3 square plates subjected to sinusoidal load (a/h=10, Type A).

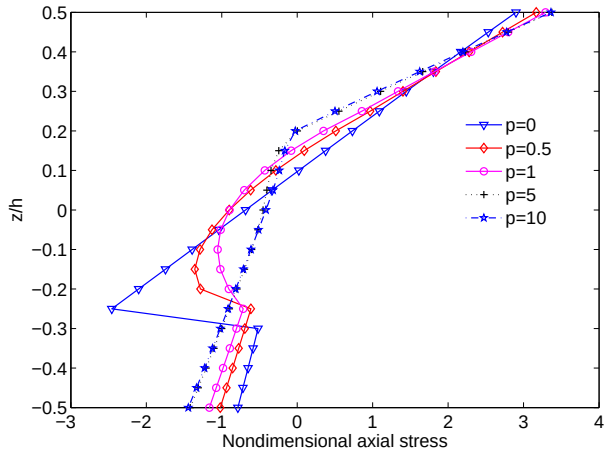

(a) $\bar{\sigma}_{xx}$ (1-2-1 Al/Al_2O_3 plate, Type B)

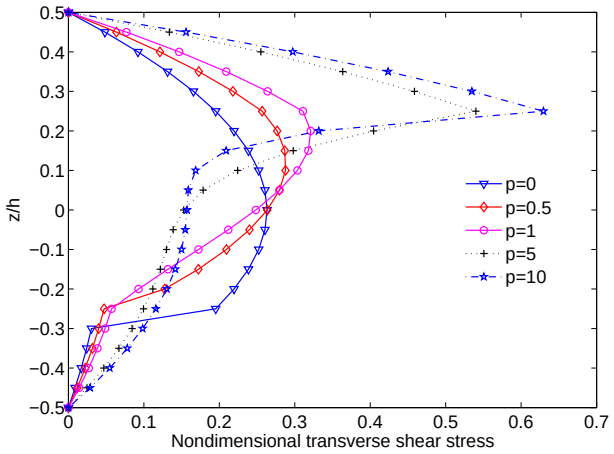

(b) $\bar{\sigma}_{xz}$ (1-2-1 Al/Al_2O_3 plate, Type B)

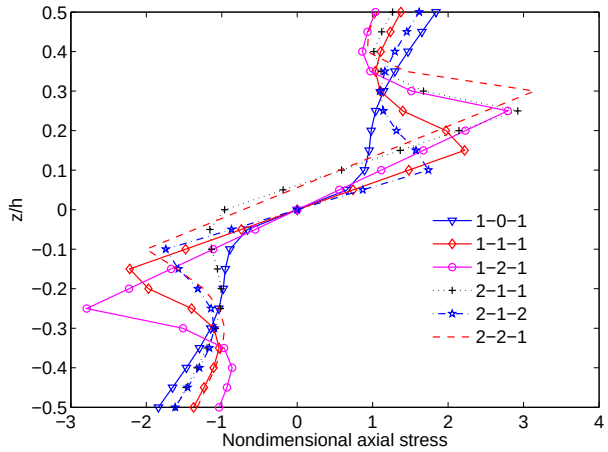

(c) $\hat{\sigma}_{xx}$ (p=5, Al/ZrO_2 plate, Type C)

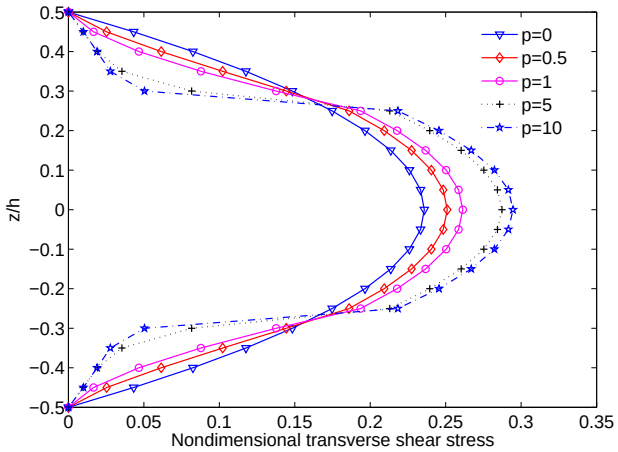

(d) $\bar{\sigma}_{xz}$ (1-2-1 Al/ZrO_2 plate, Type C)

Figure 5: Nondimensional stresses through the thickness direction for different values of p of Al/Al_2O_3 and Al/ZrO_2 square sandwich plates subjected to sinusoidal load with (a/h=10, Type B and Type C).

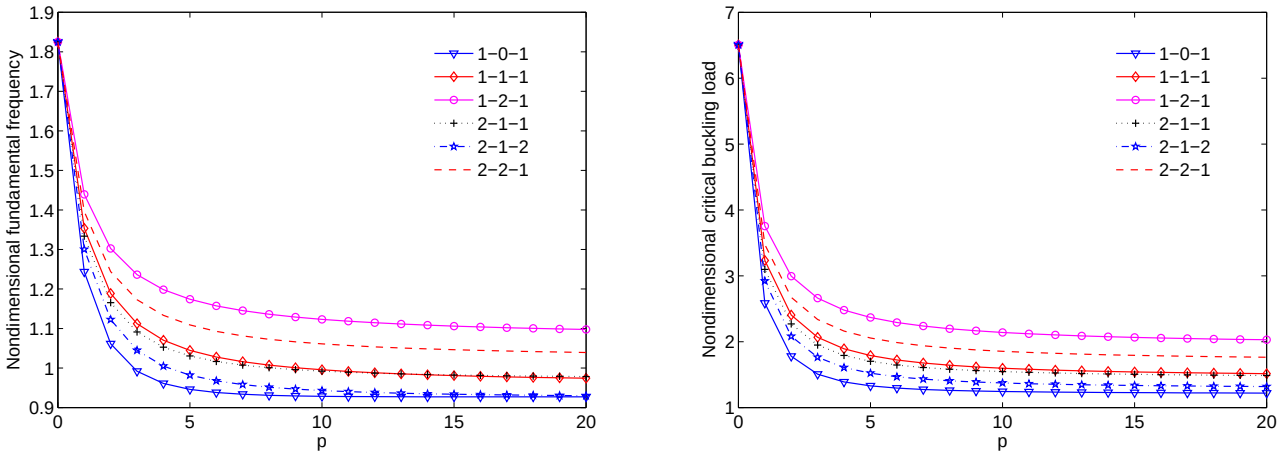

(a) (b)

Figure 6: Effect of the power-law index p on the nondimensional fundamental frequency ($\hat{\omega}$) and critical buckling load ($\hat{N}_{cr}$) of Al/Al_2O_3 square sandwich plates (a/h=10, Type C).

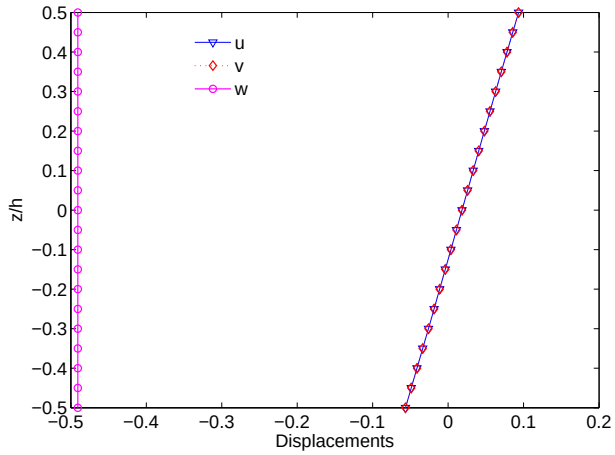

(a) Mode 1

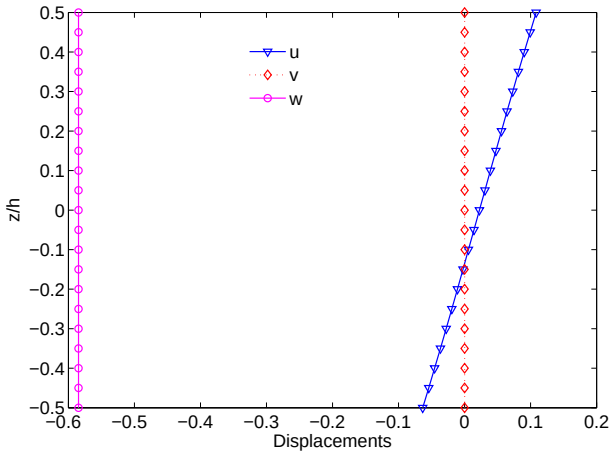

(b) Mode 2

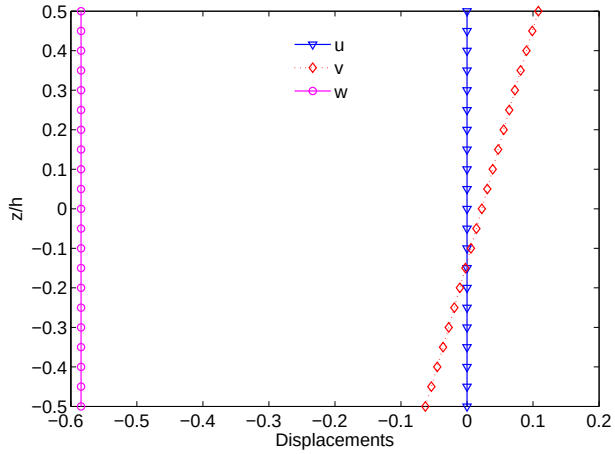

(c) Mode 3

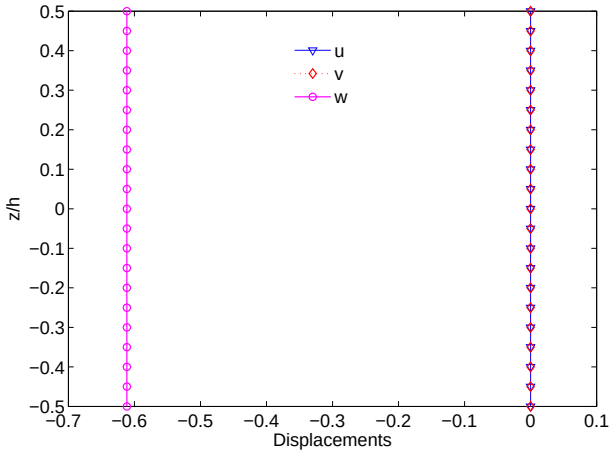

(d) Mode 4

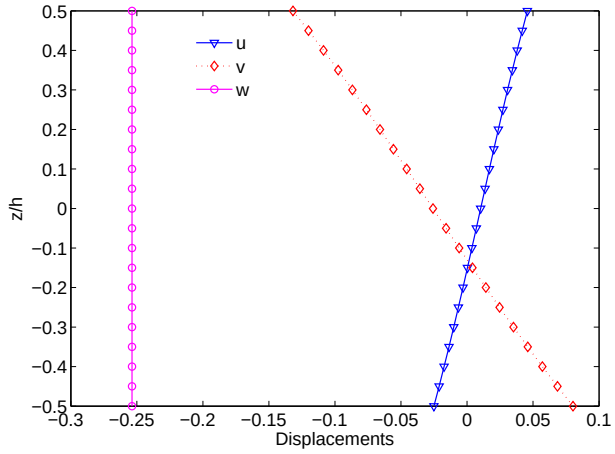

(e) Mode 5

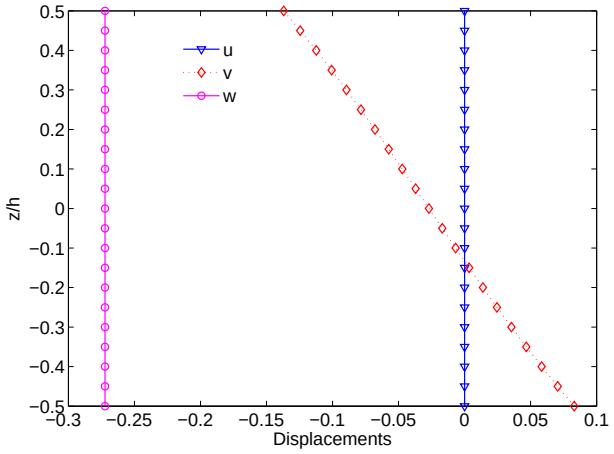

(f) Mode 6

Figure 7: Displacement shapes of six modes of (1-2-1) Al/Al_2O_3 square sandwich plates (a/h=10, p=5, x=a/4, y=b/4, Type B).